D1-82-0239

"Also available from the author"

BOEING SCIENTIFIC RESEARCH LABORATORIES

On the Acceleration of Magnetogasdynamic Channel Flows Through the Sonic Velocity

F. D. Hains

March 1963

(14) D1-82-0239

BOEING SCIENTIFIC RESEARCH LABORATORIES

FLIGHT SCIENCES LABORATORY REPORT NO. 72

(6) ON THE ACCELERATION OF MAGNETOGASDYNAMIC CHANNEL

FLOWS THROUGH THE SONIC VELOCITY

(10) by

F. D. Hains

March 1963

SYMBOLS

B	Magnetic field
E	Electric field
H	Total enthalpy
M	Mach number
m	Source strength
N	Interaction parameter
p	Pressure
r	Radial distance
R	Gas constant
R_m	Magnetic Reynolds number
T	Temperature
u,v,w	r, θ, z components of velocity, respectively
α	$\dfrac{\gamma - 1}{2\gamma}$
β	$\dfrac{N}{m}$
γ	Ratio of specific heats

ON THE ACCELERATION OF MAGNETOGASDYNAMIC CHANNEL

FLOWS THROUGH THE SONIC VELOCITY

by F. D. Hains

SUMMARY

The possibility of passage through the sonic
velocity is examined for the magnetogasdynamic flow through
a diverging, straight-walled channel. In addition to the
usual assumptions of continuum MGD, the electrical conduc-
tivity is assumed to be small, but the effect of Hall
current is included. A number of different cases arise,
depending on whether or not one or more parameters vanish
or are small.

Numerical results for the case where the Hall
current vanishes, and the problem becomes analogous to the
gasdynamic source, indicate the sonic point can be placed
anywhere along the channel by proper selection of the
electric and magnetic field strengths and boundary condi-
tions.

I. INTRODUCTION

This report deals with the flow of compressible, electrically conducting gases of sufficient density to satisfy the continuum assumptions of gasdynamics. An attempt will be made to obtain exact solutions, either closed form or numerical, of the magnetogasdynamic flow equations. Since the MGD equations reduce to those of ordinary gas dynamics when the electrical conductivity vanishes, it is logical to seek solutions which will reduce to known exact solutions of gasdynamics. Two exact solutions of gasdynamics are the source-sink and source-vortex. This report will consider the MGD source and will emphasize those solutions which pass through the sonic velocity.

In Reference 1, three simple solutions for the MGD source were presented. The configuration studied is shown in Figure 1. A source flow with radial velocity u interacts with crossed electric and magnetic field. The electric field is uniform in the z direction, while the magnetic field is produced by a wire along the z axis. The three cases considered are summarized in Table I.

TABLE I

Case	R_m	K	E	β	Comments
A	O	O	O	Finite	Closed form solution
B	O	O	Finite	O	Solution sketched
C	O	O	Finite	Finite	One particular solution

Closed form solutions were obtained in Case A, where the electric

field vanishes and the flow is isoenergetic. The velocity distributions for various values of β are shown in Figure 3. Only the solution for $\beta = 0.6$ passes through the sonic velocity $u = 0.5$. All other solutions terminate with sonic velocity at a limit circle. Some of these solutions lie inside a limit circle while others lie outside a limit circle. The solutions for Case B are sketched in Figure 4. It appears that all solutions for this case are bounded in finite regions formed by two limit circles. In Case C, a particular solution was obtained which proceeds at constant Mach number.

The cases discussed in this report are shown in Table II. Because of the non-linearity of the equations, numerical integration is usually required for these cases.

TABLE II

Case	R_m	K	E	β	Comments
1	0	Finite	Finite	Finite	
2	0	Finite	Finite	Finite	One particular solution
3	0	0	Finite	Finite	$w \neq 0$
4	0	0	Finite	Finite	$w = 0$
5	Finite	0	0	Finite	
6	Finite	0	0	0	Solve for B_θ

II. BASIC EQUATIONS

The basic MGD equations in vector form are

continuity $\qquad \vec{\nabla}\cdot\rho\vec{q} = 0$ $\qquad\qquad\qquad\qquad\qquad$ (1)

momentum $\qquad \rho(\vec{q}\cdot\vec{\nabla})\vec{q} + \vec{\nabla}p = \vec{j} \times \vec{B}$ $\qquad\qquad\qquad$ (2)

energy $\qquad \rho(\vec{q}\cdot\vec{\nabla})H = \vec{E} \cdot \vec{j}$ $\qquad\qquad\qquad\qquad$ (3)

Ohm's law $\qquad \vec{j} = \sigma\left[\vec{E} + \vec{q} \times \vec{B} - \dfrac{\vec{j}\times\vec{B}}{n_e e}\right]$ $\qquad\qquad$ (4)

Maxwell's $\qquad \vec{\nabla} \cdot \vec{j} = 0$ $\qquad\qquad\qquad\qquad\qquad\qquad$ (5)
equations

$\qquad\qquad\qquad \vec{j} = \vec{\nabla} \times \vec{B}$ $\qquad\qquad\qquad\qquad\qquad\qquad$ (6)

$\qquad\qquad\qquad \vec{\nabla} \cdot \vec{B} = 0$ $\qquad\qquad\qquad\qquad\qquad\qquad$ (7)

$\qquad\qquad\qquad \vec{\nabla} \times \vec{E} = 0$ $\qquad\qquad\qquad\qquad\qquad\qquad$ (8)

$\qquad\qquad\qquad \vec{\nabla} \cdot \vec{E} = 0$ $\qquad\qquad\qquad\qquad\qquad\qquad$ (9)

gas law $\qquad p = \rho R T$ $\qquad\qquad\qquad\qquad\qquad\qquad$ (10)

Equations (1) – (9) can be expressed in the following scalar form in
the r-θ-z coordinate system of Figure 1.

$$\frac{1}{r}\frac{\partial}{\partial r}(r\rho u) + \frac{1}{r}\frac{\partial}{\partial \theta}(\rho v) + \frac{\partial}{\partial z}(\rho w) = 0 \qquad\qquad (11)$$

$$\rho\left[u\frac{\partial u}{\partial r} + \frac{v}{r}\frac{\partial u}{\partial \theta} - \frac{v^2}{r} + w\frac{\partial u}{\partial z}\right] + \frac{\partial p}{\partial r} = j_\theta B_z - j_z B_\theta \qquad\qquad (12)$$

$$\rho\left[u\frac{\partial v}{\partial r} + \frac{v}{r}\frac{\partial v}{\partial \theta} + \frac{uv}{r} + w\frac{\partial v}{\partial z}\right] + \frac{\partial p}{\partial \theta} = j_z B_r - j_r B_z \qquad\qquad (13)$$

$$\rho\left[u\frac{\partial w}{\partial r} + \frac{v}{r}\frac{\partial w}{\partial \theta} + w\frac{\partial w}{\partial z}\right] + \frac{\partial p}{\partial z} = j_r B_\theta - j_\theta B_r \qquad\qquad (14)$$

$$\rho u \frac{\partial H}{\partial r} + \frac{\rho v}{r} \frac{\partial H}{\partial \theta} + \rho w \frac{\partial H}{\partial z} = E_r j_r + E_\theta j_\theta + E_z j_z \tag{15}$$

$$j_r = \sigma \left[E_r + v B_z - w B_\theta - \frac{1}{n_e e}(j_\theta B_z - j_z B_\theta) \right] \tag{16}$$

$$j_\theta = \sigma \left[E_\theta + w B_r - u B_z - \frac{1}{n_e e}(j_z B_r - j_r B_z) \right] \tag{17}$$

$$j_z = \sigma \left[E_z + u B_\theta - v B_r - \frac{1}{n_e e}(j_r B_\theta - j_\theta B_r) \right] \tag{18}$$

$$\frac{1}{r} \frac{\partial}{\partial r}(r j_r) + \frac{1}{r} \frac{\partial j_\theta}{\partial \theta} + \frac{\partial j_z}{\partial z} = 0 \tag{19}$$

$$j_r = \frac{1}{r} \left(\frac{\partial B_r}{\partial \theta} - \frac{\partial r B_\theta}{\partial z} \right) \tag{20}$$

$$j_\theta = \frac{1}{r} \left(\frac{\partial B_r}{\partial z} - \frac{\partial B_z}{\partial r} \right) \tag{21}$$

$$j_z = \frac{1}{r} \left(\frac{\partial r B_\theta}{\partial r} - \frac{\partial B_r}{\partial \theta} \right) \tag{22}$$

$$\frac{1}{r} \frac{\partial}{\partial r}(r B_r) + \frac{1}{r} \frac{\partial B_\theta}{\partial \theta} + \frac{\partial B_z}{\partial z} = 0 \tag{23}$$

$$\frac{\partial E_r}{\partial \theta} - \frac{\partial r E_\theta}{\partial z} = 0 \tag{24}$$

$$\frac{\partial E_r}{\partial z} - \frac{\partial E_z}{\partial r} = 0 \tag{25}$$

$$\frac{\partial r E_\theta}{\partial r} - \frac{\partial E_r}{\partial \theta} = 0 \tag{26}$$

$$\frac{1}{r} \frac{\partial r E_r}{\partial r} + \frac{1}{r} \frac{\partial E_\theta}{\partial \theta} + \frac{\partial E_z}{\partial z} = 0 \tag{27}$$

To obtain solutions to this set of equations without further simplifying assumptions would be difficult.

For the source shown in Figure 1, we can assume

$$B_r = B_z = E_r = E_\theta = \frac{\partial}{\partial \theta} = 0$$

$$E_z = E \qquad \text{(a constant)}$$

(28)

Eqs. (23) – (27) are automatically satisfied by these assumptions. In addition, Eq. (13) is satisfied by $v = 0$, and Eq. (21) leads to $j_\theta = 0$. The remaining equations simplify to

$$\frac{1}{r} \frac{\partial}{\partial r}(r\rho u) + \frac{\partial}{\partial z}(\rho w) = 0$$

(29)

$$\rho \left[u \frac{\partial u}{\partial r} + w \frac{\partial u}{\partial z} \right] + \frac{\partial p}{\partial r} = -j_z B_\theta$$

(30)

$$\rho \left[u \frac{\partial w}{\partial r} + w \frac{\partial w}{\partial z} \right] + \frac{\partial p}{\partial z} = j_r B_\theta$$

(31)

$$\rho u \frac{\partial H}{\partial r} + \rho w \frac{\partial H}{\partial z} = E j_z$$

(32)

$$j_r = \sigma \left[-w B_\theta + \frac{1}{n_e e}(j_z B_\theta) \right]$$

(33)

$$j_z = \sigma \left[E + u B_\theta - \frac{1}{n_e e}(j_r B_\theta) \right]$$

(34)

$$\frac{1}{r} \frac{\partial}{\partial r}(r j_r) + \frac{\partial j_z}{\partial z} = 0$$

(35)

$$j_r = -\frac{1}{r} \frac{\partial}{\partial z}(r B_\theta)$$

(36)

$$j_z = \frac{1}{r}\frac{\partial}{\partial r}(rB_\theta) \tag{37}$$

Combining Eq. (33) and (34)

$$j_r = \frac{\sigma}{1 + \left(\dfrac{\sigma B_\theta}{n_e e}\right)^2}\left[-wB_\theta + \frac{\sigma B_\theta}{n_e e}(E + uB_\theta)\right] \tag{38}$$

and

$$j_z = \frac{\sigma}{1 + \left(\dfrac{\sigma B_\theta}{n_e e}\right)^2}\left[E + uB_\theta + \frac{\sigma B_\theta^2 w}{n_e e}\right] \tag{39}$$

These two equations are used to eliminate j_r and j_z from the other equations.

All equations up to this point are dimensional, although the tilda which indicates a dimensional quantity has been omitted for simplicity. It is convenient at this point to non-dimensionalize, using the following definitions:

$$
\left.
\begin{aligned}
&r = \tilde{r}/r_o && \rho = \tilde{\rho}/\rho_s && u = \tilde{u}/u_m && p = \tilde{p}/p_s \\[2mm]
&z = \tilde{z}/r_o && T = \tilde{T}/T_s && w = \tilde{w}/u_m && B_\theta = \tilde{B}_\theta/B_o \\[2mm]
&j_r = \tilde{j}_r/\sigma u_m B_o && j_z = \tilde{j}_z/\sigma u_m B_o && E = \tilde{E}/u_m B_o && H = \tilde{H}\Big/\frac{\gamma}{\gamma-1}\frac{p_s}{\rho_s} \\[2mm]
&R_m = \tilde{\sigma} u_m r_o && N = \frac{\tilde{\sigma}B_o^2 r_o}{\rho_s u_m} && K = \frac{\tilde{\sigma}B_o}{\tilde{n}_e \tilde{e}} && m = \tilde{m}/r_o \rho_s u_m
\end{aligned}
\right\} \tag{40}
$$

Many of these are the same used in Case A of Reference 1 where the flow is isoenergetic ($E = 0$) so that

$$\frac{\gamma}{\gamma-1}\frac{p_s}{\rho_s} = \frac{u_m^2}{2} \tag{41}$$

Although E is generally not zero in this report, it is convenient to retain the same definitions.

The non-dimensional form of the basic equations is

$$\frac{1}{r}\frac{\partial}{\partial r}(r\rho u) + \frac{\partial}{\partial z}(\rho w) = 0 \tag{42}$$

$$\rho u \frac{\partial u}{\partial r} + \rho w \frac{\partial u}{\partial z} + \alpha \frac{\partial p}{\partial r} = \frac{-NB_\theta\left[E+uB_\theta+KwB_\theta^2\right]}{1+K^2B_\theta^2} \tag{43}$$

$$\rho u \frac{\partial w}{\partial r} + \rho w \frac{\partial w}{\partial z} + \alpha \frac{\partial p}{\partial z} = \frac{NB_\theta^2\left[-w+K(E+uB_\theta)\right]}{1+K^2B_\theta^2} \tag{44}$$

$$\rho u \frac{\partial H}{\partial r} + \rho w \frac{\partial H}{\partial z} = \frac{2NE(E+uB_\theta+KwB_\theta^2)}{1+K^2B_\theta^2} \tag{45}$$

$$R_m\left[\frac{1}{r}\frac{\partial}{\partial r}\left(\frac{rB_\theta\left(-w+K\left[E+uB_\theta\right]\right)}{1+K^2B_\theta^2}\right) + \frac{\partial}{\partial z}\frac{E+uB_\theta+KwB_\theta^2}{1+K^2B_\theta^2}\right] = 0 \tag{46}$$

$$\frac{1}{r}\frac{\partial}{\partial z}(rB_\theta) = \frac{R_m\left[wB_\theta-KB_\theta(E+uB_\theta)\right]}{1+K^2B_\theta^2} \tag{47}$$

$$\frac{1}{r}\frac{\partial}{\partial r}(rB_\theta) = \frac{R_m\left[E+uB_\theta+KwB_\theta^2\right]}{1+K^2B_\theta^2} \tag{48}$$

where

$$p = \rho T \tag{49}$$

and

$$H = T + u^2 + w^2 \tag{50}$$

III. CASE 1

In most applications of MGD channel flow the electrical conductivity is small. For this reason this case will be restricted to solutions with $R_m = 0$. Physically this means the magnetic field will interact with the flow, but not vice versa. The basic equations simplify with Eqs. (47) and (48) satisfied by $B_\theta = 1/r$, and the remaining equations become

$$\frac{1}{r} \frac{\partial}{\partial r}(r\rho u) + \frac{\partial}{\partial z}(\rho w) = 0 \tag{51}$$

$$\rho u \frac{\partial u}{\partial r} + \rho w \frac{\partial u}{\partial z} + \alpha \frac{\partial p}{\partial r} = \frac{-N[Er + u + Kw/r]}{r^2 + K^2} \tag{52}$$

$$\rho u \frac{\partial w}{\partial r} + \rho w \frac{\partial w}{\partial z} + \alpha \frac{\partial p}{\partial z} = \frac{N[-w + K(E + u/r)]}{r^2 + K^2} \tag{53}$$

$$\rho u \frac{\partial H}{\partial r} + \rho w \frac{\partial H}{\partial z} = \frac{2NEr[Er + u + Kw/r]}{r^2 + K^2} \tag{54}$$

In this form the equations are still very difficult to solve, so we assume $\frac{\partial}{\partial z} = 0$, and reduce to the following set of ordinary differential equations

$$r\rho u = m \tag{55}$$

$$\rho u \frac{du}{dr} + \alpha \frac{dp}{dr} = \frac{-N[Er + u + Kw/r]}{r^2 + K^2} \tag{56}$$

$$\rho u \frac{dw}{dr} = \frac{N[-w + K(E + u/r)]}{r^2 + K^2} \tag{57}$$

$$\rho u \frac{dH}{dr} = \frac{2NEr[Er + u + Kw/r]}{r^2 + K^2} \tag{58}$$

Using Eqs. (49), (50) and (55) to eliminate p, ρ, and H, we obtain

$$\frac{du}{dr} = \frac{F}{G} \tag{59}$$

where

$$F \equiv u\left\{\beta\left[-\frac{2\gamma}{\gamma-1}\, r^2 u^2 - \left(\frac{4\gamma-2}{\gamma-1}\, Er^3 + \frac{2}{\gamma-1}\, Kwr\right)u - 2E^2 r^4 - 2r^2 w^2\right] + (r^2+K^2)T\right\} \tag{60}$$

$$G \equiv r(r^2+K^2)\left[\frac{2}{\gamma-1}\, u^2 - T\right] \tag{61}$$

$$\frac{dw}{dr} = \frac{\beta[-wr + K(Er + u)]}{(r^2+K^2)} \tag{62}$$

$$\frac{dT}{dr} = \frac{2\beta Er^2[Er + u + Kw/r]}{r^2+K^2} - 2u\,\frac{du}{dr} - 2w\,\frac{dw}{dr} \tag{63}$$

For given boundary conditions and specific values of the parameters γ, β, E and K, these equations can be integrated numerically to yield the solution.

Before doing this, it is interesting to study the limit circle where $F \neq 0$, $G = 0$. Eq. (59) indicates the gradient in u is infinite so the solution cannot penetrate the limit circle. From the definition of local Mach number given by

$$M = \sqrt{\left(\frac{2}{\gamma-1}\right)\frac{u^2 + w^2}{T}} \tag{64}$$

the flow must be supersonic at the limit circle. As in Case A shown in Figure 3, we expect solutions which lie inside the limit circles, and others which lie outside the limit circles. The type of results that might be expected are sketched in Figure 5(a) - 5(d).

In this report we seek solutions which do not terminate in limit lines. A characteristic point (r_c, u_c, T_c, w_c) is one which satisfies the conditions $F = G = 0$. Since $\frac{du}{dr}$ is indeterminate, more than one integral curve may pass through the characteristic point. The singularity condition $G = 0$ leads to

$$T_c = \frac{2}{\gamma-1} u_c^2 \tag{65}$$

and the regularity condition $F = 0$ leads to the expression

$$\beta\left\{\gamma U^2 + (2\gamma-1+\lambda W)U + (\gamma-1)(1+W^2)\right\} - (1+\lambda^2)U^2 = 0 \tag{66}$$

In the last equation one variable has been eliminated by introducing the quantities

$$U = \frac{u_c}{Er_c} \qquad\qquad W = \frac{w_c}{Er_c} \qquad\qquad \lambda = \frac{K}{r_c} \tag{67}$$

The slopes of the integral curves at the characteristic point are found by L'Hospital's Rule.

$$\left(\frac{du}{dr}\right)_c = \lim_{r \to r_c} \frac{du}{dr} = \lim_{r \to r_c} \frac{dF/dr}{dG/dr} \tag{68}$$

Two curves pass through each characteristic point with slopes

$$\left(\frac{du}{dr}\right)_c = \frac{-b \pm \sqrt{b^2 - 4ac}}{2a} \tag{69}$$

where

$$a = 2r_c\left(r_c^2 + K^2\right)\left(\frac{\gamma+1}{\gamma-1}\right)u_c \tag{70}$$

$$b = \left[\frac{4\gamma}{\gamma-1}\beta r_c^2 + 2r_c^2 + 2K^2\right]u_c^2 + \frac{2\gamma}{\gamma-1}\beta\left[Er_c^3 + Kw_c r_c\right]u_c - 2\beta r_c^2 w_c^2 - 2\beta E^2 r_c^4 \quad (71)$$

$$c = \frac{2}{(\gamma-1)(r_c^2+K^2)}\left[2(\gamma\beta-1)r_c^3 + (2\beta\gamma + \beta^2 - 2)r_c K^2\right]u_c^3$$

$$+ \frac{2}{(\gamma-1)(r_c+K^2)}\left[(5\gamma-2)\beta Er_c^4 + (5\gamma-2+\beta)\beta EK^2 r_c^2 + (\gamma+2\beta\gamma-3\beta)\beta Kr_c^2 w_c\right.$$

$$\left. + \gamma\beta K^3 w_c\right]u_c^2 + \frac{2\beta}{r_c^2+K^2}\left[3E^2 r_c^5 + 3E^2 K^2 r_c^3 + \left(r_c^3+r_c K^2 - 2\beta r_c^3\right)w_c^2\right.$$

$$\left. + 2\beta KEr_c^3 w_c\right]u_c \quad (72)$$

If, for example, r_c and u_c are specified, the other coordinates T_c and w_c of the characteristic point are found from Eqs. (65) and (66), respectively. The slopes of the two solutions are then found from Eq. (69). This information is sufficient to start integration of Eqs. (59), (62) and (63) at the characteristic point in both the upstream and downstream directions.

In Reference 2, a study is made of an accelerator similar to the one shown in Figure 2. The electrodes are assumed to be parallel to the r-θ plane so that at these surfaces w = 0. Eqs. (59) and (63) were solved for supersonic flows with the assumption w = 0 everywhere. It is claimed this is a reasonable approximation as long as K < 1. The real criteria should be how large is the term $\frac{\beta K(Er+u)}{r^2 + K^2}$ in Eq. (62). Even if K < 1 this term might be large and make the approximation a poor one. In order to obtain an exact solution one must return to the set of Eqs. (51)-(54) which allow for a variation in the z direction.

IV. **CASE 2**

The non-dimensional forms of Eqs. (38) and (39) are

$$j_r = \frac{1}{r^2 + K^2}\left[-wr + K(Er + u)\right] \tag{73}$$

$$j_z = \frac{1}{r^2 + K^2}\left[Er^2 + w + Kw\right] \tag{74}$$

The introduction of w and the Hall current usually results in a radial component of current. If we specify that

$$w = \frac{K(Er + u)}{r} \tag{75}$$

so that $j_r = 0$, Eqs. (59), (62) and (63) are satisfied by the solution

$$u = \frac{-NE}{N + m}\,r \tag{76}$$

$$w = \frac{KE}{\beta + 1} \tag{77}$$

$$p = \frac{-E^2 m}{\beta + 1} \tag{78}$$

$$\rho = -\frac{m(\beta + 1)}{\beta E r^2} \tag{79}$$

The Mach number is constant

$$M = \left(\frac{2}{\gamma - 1}\right)\beta \tag{80}$$

This particular solution reduces to Case C when K = 0.

V. CASE 3

If $K = 0$, Eqs. (59)-(63) reduce to

$$\frac{du}{dr} = \frac{u\left\{\beta\left[-\frac{2\gamma}{\gamma-1}u^2 - \frac{4\gamma-2}{\gamma-1}Eru - 2E^2r^2 - 2w^2\right] + T\right\}}{r\left(\frac{2}{\gamma-1}u^2 - T\right)} = \frac{F}{G} \tag{81}$$

$$w = c_1 r^{-\beta} \tag{82}$$

$$\frac{dT}{\partial r} = 2\beta E[Er + u] - 2u\frac{du}{dr} - 2w\frac{dw}{dr} \tag{83}$$

where c_1 is a constant of integration. With the Hall current absent, solutions can still be obtained with $j_r \neq 0$. The numerical integration of these equations is treated in the same way as in Case 1.

VI. CASE 4

If $c_1 = 0$, so that $w = 0$, Eqs. (81) and (83) become

$$\frac{du}{dr} = \frac{-u\beta\left[\frac{2\gamma}{\gamma-1}u^2 + \frac{4\gamma-2}{\gamma-1}Eru + 2E^2r^2\right] + uT}{r\left[\frac{2}{\gamma-1}u^2 - T\right]} \tag{84}$$

$$\frac{dT}{dr} = 2\beta E(Er + u) - 2u\frac{du}{dr} \tag{85}$$

In this case, the flow velocity is in the radial direction and the electrodes shown in Figure 2 are planes perpendicular to the wire. It is convenient to split this problem into two subcases, depending on the sign of E.

If $E < 0$, the introduction of the similarity parameter*

$$\zeta = - Er \tag{86}$$

leads to

$$\frac{du}{d\zeta} = \frac{\beta\left[-\frac{2\gamma}{\gamma-1}u^3 + \frac{4\gamma-2}{\gamma-1}\zeta u^2 - 2\zeta^2 u\right] + uT}{\zeta\left(\frac{2}{\gamma-1}u^2 - T\right)} \equiv \frac{F}{G} \tag{87}$$

$$\frac{dT}{dr} = 2\beta(\zeta - u) - 2u\frac{du}{d\zeta} \tag{88}$$

Again we restrict our interest to solutions that do not terminate in

---

* The similarity parameters $U = \frac{-u}{E}$ and $t = \frac{T}{E^2}$ could also be used. These parameters are used in the treatment of the constant area channel in Appendix A.

limit lines. Since $w = 0$, the flow is sonic at the limit circle, so the solutions we seek must pass through the sonic velocity.

The singularity condition $G = 0$ is the same as Eq. (65), while the regularity condition $F = 0$ leads to

$$\frac{u_c}{\zeta_c} = \frac{1 - 2\gamma \pm \sqrt{\frac{4(\gamma-1)}{\beta} + 1}}{2(\gamma - \frac{1}{\beta})} \equiv \psi \tag{89}$$

The two roots ψ_1 and ψ_2 are plotted as a function of β in Figure 6 for a monatomic gas. Only positive values of ψ are plotted since u_c must be positive. For this reason ψ_2 is not shown for $\beta < 0.6$. The graph shows that $0 \leq \psi_1 \leq 0.4$ and $1.0 < \psi_2$.

Eq. (89) shows the locus of the projection of the characteristic points (ζ_c, u_c, T_c) on the u_c-ζ_c plane is a straight line for each value of β. Some of these lines are shown in Figure 7. No characteristic points lie in the region separated by the lines $\beta = \infty$.

Following the method used in Case 1, the slopes of the two solutions passing through a characteristic point are

$$\left(\frac{du}{d\zeta}\right)_c = \frac{-b \pm \sqrt{b^2 - 4ac}}{2a} \tag{90}$$

where

$$\left. \begin{aligned} a &= 8\psi \\ b &= (15\beta - 1)\psi^2 - 12\beta\psi \\ c &= (2 - 5\psi)\beta\psi \end{aligned} \right\} \tag{91}$$

For each value of ψ, two values of $(du/d\zeta)_c$ are obtained. The slopes

are a function of β only, and hence are constant along each of the straight lines in Figure 7. The variation of slope with β is shown in Figure 8. Only one of the four curves is negative, so that most of the solutions are accelerating flows. The curves corresponding to Ψ_2 terminate at $\beta = 0.6$ where Ψ_2 is infinite, and the curves corresponding to Ψ_1 terminate at $\beta = 0.3$ where the slopes become complex. These results are shown in Figure 7.

Numerical solutions were obtained for $\zeta_c = 1.0$ and $\beta = 2.0$. The results are compared with the ordinary gasdynamic flow $E = B = 0$ in Table III.

TABLE III

	u	T	M	ρ/m	p/m
	Fig. 9	Fig. 10	Fig. 11	Fig. 12	Fig. 13
E = B = 0	↑	↓	↑	↓	↓
	↓	↑	↓	↑	↑
———	↑	↑	↑	↓	↓
– – – – –	↑	↑	↓	↓	↑
– – –	↑	↓Min↑	↑Max↓	↓	↓
━━━━	↓Min↑	↑	↓	↑Max↓	↑

The solid curve in Figures 9 - 13 corresponds to an accelerating flow which becomes asymptotic to the solution given by

Eqs. (76) - (80) in Case 2 with K = 0. The solution begins at a finite radius with infinite density, finite pressure, and zero velocity, temperature and Mach number. Energy is continuously fed into the gas as it accelerates through the sonic velocity.

The solution shown by the dashed curves is an accelerating flow whose temperature and pressure increases as the Mach number and density decreases. The solution begins with zero pressure and density, and finite velocity, temperature and Mach number. As the velocity increases, the rapid rise in temperature causes a drop in the Mach number until the initially supersonic flow becomes subsonic. Again energy is continuously added to the gas, but at any point in the flow this solution has a higher stagnation enthalpy than the previous one.

The dot-dashed curves begin at $\zeta = 0$ with infinite pressure and density, and finite velocity, temperature and Mach number. The flow accelerates through the sonic velocity and becomes asymptotic to the solution for Case 2. In order to accomplish this, a minimum occurs in the temperature curve and a maximum in the Mach number curve. Energy is extracted from the flow up to $\zeta = 2.2$ and added to the flow beyond that point. Thus, the flow acts first as a generator and then later as a motor.

The solution plotted as heavy dashed curves is the only decelerating flow at the sonic point. The flow begins at a finite radius with zero temperature and pressure, and finite velocity, density and Mach number. The supersonic flow decelerates through the sonic velocity, reaches a minimum velocity, and begins to accelerate. The density reaches a maximum while the flow is still decelerating. The flow

changes from a generator to a motor after passing the sonic point.

The second subcase occurs when $E > 0$. Introducing the similarity parameter

$$\zeta = Er$$

Eqs. (84) and (85) become

$$\frac{du}{d\zeta} = \frac{-\beta\left[\frac{2\gamma}{\gamma-1}u^3 + \frac{4\gamma-2}{\gamma-1}\zeta u^2 + 2\zeta^2 u\right] + uT}{\zeta\left[\frac{2}{\gamma-1}u^2 - T\right]} \qquad (92)$$

$$\frac{dT}{d\zeta} = 2\beta(\zeta + u) - 2u\frac{du}{d\zeta} \qquad (93)$$

Following the procedure used in the first subcase,

$$\frac{u_c}{\zeta_c} = \frac{-1 + 2\gamma \pm \sqrt{\frac{4(\gamma-1)}{\beta} + 1}}{2\left(\gamma - \frac{1}{\beta}\right)} \equiv \varphi \qquad (94)$$

$$\left(\frac{du}{d\zeta}\right)_c = \frac{-b \pm \sqrt{b^2 - 4ac}}{2a} \qquad (95)$$

where

$$\left.\begin{aligned} a &= 8\varphi \\[1em] b &= (15\beta - 1)\varphi^2 + 12\beta\varphi \\[1em] c &= (2 + 5\varphi)\beta\varphi \end{aligned}\right\} \qquad (96)$$

The variation of the quantity φ appearing in Eq. (94) is shown in

Figure 6. This quantity is positive only if $\beta < 0.6$, and takes on all positive values. Hence, all points in the u-ζ plane can be characteristic points. The slopes of the solutions at the characteristic points are plotted in Figure 14 as a function of β. The slopes are both negative and are real for $0.32 < \beta < 0.60$. The locus of possible characteristic points which yield real solutions are shown in Figure 15.

Numerical solutions were obtained for $\zeta_c = 1.0$ and $\beta = 0.5$. These results appear in Figures 16-20. Only curve I is shown because an infinite number of curves pass through the characteristic point with the same slope as curve II, which is the envelope of the curves. The numerical integration in a direction away from the characteristic point was found to be unstable while integration towards the characteristic point was stable. Two solutions called IIa and IIb are shown in Figures 21-25 for a small region near the characteristic point. Away from the characteristic point these solutions are practically the same as curve I and cannot be distinguished in the scales used in Figures 16-19. No attempt was made to extend the envelope II or to extend the curves IIa and IIb into the region where $\zeta < 1$.

Curve I begins at a finite radius with zero temperature and pressure, and infinite Mach number. The velocity and density are finite. As the flow decelerates through the sonic velocity the temperature and pressure increases as the density decreases. Energy is added to the flow for all solutions with $E > 0$.

The reason why an infinite number of solutions must pass through the characteristic point is that both curves I and II are decelerating and supersonic when $\zeta < \zeta_c$, and both decelerating and

subsonic when $\zeta > \zeta_c$. This means they pass from region 1 to region 3 in Figure 26. The curve AC is the locus of characteristic points, or the intersection of the surface $F = 0$ with the sonic surface $G = 0$. In regions 1 and 2 above the sonic surface the flow is supersonic, and in regions 3 and 4 below the sonic surface the flow is subsonic. The curves I and II intersect at the characteristic point B. The surface E is generated by curve I as B moves from A to C and the surface D is a similar surface generated by curve II. Solutions which pass through points in region 1 lying between surfaces D and E must pass through the curve AC with the two permissible slopes of curves I and II. The solutions cannot penetrate the surfaces D or E except along AC, for this would produce a characteristic point which can occur only along AC. Neither can they be parallel to AC because the projection A'B' on the u-ζ plane has a positive slope while $\frac{du}{d\zeta} < 0$ in region 1. Thus, as numerical integration shows, curve II is an envelope of solutions such as IIa and IIb which pass through the characteristic point with the same slope.

In all the cases for $E < Q$, which are shown in Figure 9, the two curves passing through the characteristic point are always separated by a sonic surface and the surface $F = 0$ for any given value of ζ. Thus, at the same ζ one solution is subsonic while the other is supersonic. This means the surfaces corresponding to D and E in Figure 26 always lie in different regions, and only two curves can pass through the characteristic point.

Some solutions for accelerating supersonic flows were presented in Reference 3. One type of solution is asymptotic to Case 2

with K = 0. The second type of solution accelerates to a maximum
velocity and then decelerates and terminates at a limit line. No
solutions for acceleration through the sonic velocity were presented.

VII. CASE 5

This case deals with solutions for finite values of R_m. First, the method of small perturbations is used to find solutions which hold for small values of R_m. The one solution of Case A which passes through the sonic velocity is chosen as the zero order solution.

Let

$$
\left.
\begin{aligned}
u &= u_o + R_m u_1 + R_m^2 u_2 + \cdots \\
p &= p_o + R_m p_1 + R_m^2 p_2 + \cdots \\
\rho &= \rho_o + R_m \rho_1 + R_m^2 \rho_2 + \cdots \\
B_\theta &= \left(B_\theta\right)_o + R_m \left(B_\theta\right)_1 + R_m^2 \left(B_\theta\right)_2 + \cdots
\end{aligned}
\right\} \tag{97}
$$

With $E = \dfrac{\partial}{\partial z} = 0$, Eqs. (42)-(50) reduce to

$$
r\rho u = m \tag{98}
$$

$$
\rho u \frac{du}{dr} + \alpha \frac{dp}{dr} = -NuB_\theta^2 \tag{99}
$$

$$
p + \rho u^2 = \rho \tag{100}
$$

$$
\frac{dB_\theta}{dr} + \frac{B_\theta}{r} = R_m u B_\theta \tag{101}
$$

Substitution of Eq. (97) into Eqs. (98)-(101) and collection of like powers of R_m yields:

$$\left(R_m^o\right)$$

$$
r\rho_o u_o = m \tag{102}
$$

$$
\rho_o u_o \frac{du_o}{dr} + \alpha \frac{dp_o}{dr} = -Nu_o\left(B_\theta\right)_o^2 \tag{103}
$$

$$p_o + \rho_o u_o^2 = \rho_o \tag{104}$$

$$\frac{d\left(B_\theta\right)_o}{dr} + \frac{\left(B_\theta\right)_o}{r} = 0 \tag{105}$$

$$\left(R_m^1\right)$$

$$\rho_1 u_o + \rho_o u_1 = 0 \tag{106}$$

$$\rho_o u_o \frac{du_1}{dr} + \left(\rho_o u_1 + \rho_1 u_o\right)\frac{du_o}{dr} + \alpha\,\frac{dp_1}{dr} =$$

$$-N\left[u\left(B_\theta\right)_o^2 + 2u_o\left(B_\theta\right)_o\left(B_\theta\right)_1\right] \tag{107}$$

$$p_1 + 2\rho_o u_o u_1 + \rho_1 u_o^2 = \rho_1 \tag{108}$$

$$\frac{d\left(B_\theta\right)_1}{dr} + \frac{\left(B_\theta\right)_1}{r} = u_o\left(B_\theta\right)_o \tag{109}$$

In this analysis the higher order terms will be neglected.

The zero order equations (102)-(106) are satisfied by the solution of Case A with $\beta = \gamma^{-1}$.

$$u_o = \frac{1}{R}$$

$$\rho_o = 1$$

$$\left(B_\theta\right)_o = \frac{1}{mR} \tag{110}$$

$$p_o = \left(1 - \frac{1}{R^2}\right)$$

$$R \equiv \frac{r}{m}$$

Combining Eqs. (106) and (108),

$$p_1 = -\left(R + \frac{1}{R}\right) u_1 \tag{112}$$

and integration of Eq. (109) leads to

$$\left(B_\theta\right)_1 = \frac{\ln C_1 R}{R} \tag{113}$$

where C_1 is the integration constant. Elimination of p_1 and $\left(B_\theta\right)_1$ from Eq. (107) yields

$$\frac{d(Ru_1)}{dR} = \frac{-4\ln C_1 R}{R\left[(\gamma+1)-(\gamma-1)R^2\right]} \equiv \frac{F}{G} \tag{114}$$

The singularity condition $G = 0$ is

$$R_c = \sqrt{\frac{\gamma+1}{\gamma-1}} \tag{115}$$

and the Regularity condition $F = 0$ is

$$C_1 = \sqrt{\frac{\gamma-1}{\gamma+1}} \tag{116}$$

Integration of Eq. (114) results in

$$u_1 = \frac{-4}{(\gamma+1)R} \int_{\sqrt{\frac{\gamma-1}{\gamma+1}}}^{\sqrt{\frac{\gamma-1}{\gamma+1}}\,R} \frac{\ln x}{x(1-x^2)}\, dx \tag{117}$$

The variation of $\left(B_\theta\right)_1$, u_1, ρ_1 and p_1 with R when $\gamma = 5/3$ is shown in Figure 27. $\left(B_\theta\right)_1$ is negative upstream of the sonic point, and zero at the sonic point. Downstream of the sonic point it is positive,

and reaches a maximum at $R = 2e$. The curve for u_1 increases rapidly from zero to a maximum at the sonic point. The perturbation in pressure and the perturbation in density decreases from zero to $- 2.5$.

The previous method is valid only for small values of the magnetic Reynolds number. The application of the method to some other solutions of Case A other than the one with $\beta = \gamma^{-1}$ is difficult because of the complicated form of the zero order solution. For these reasons an attempt is made to solve Eqs. (98)-(101) directly for finite values of R_m. The numerical approach of Case 4 is used.

Integration of Eq. (101) yields

$$B_\theta = \frac{1}{r} \exp\left[R_m \int_{r_i}^{r} u \, dr\right] \tag{118}$$

As will be shown later, all solutions passing through the sonic velocity are decelerating so that r_i is either zero or the place where $u = 1$. Elimination of the density and pressure from the momentum equation results in the expression

$$\frac{du}{dr} = \frac{-\beta r^2 u^3 B_\theta^2 + \left(\frac{\gamma-1}{2\gamma}\right) u(1-u^2)}{r\left[u^2 - \left(\frac{\gamma-1}{2\gamma}\right)(1+u^2)\right]} \tag{119}$$

Restricting our attention to $\gamma = 5/3$, and substituting Eq. (118) for B_θ,

$$\frac{du}{dr} = \frac{-5u^3 \beta \exp\left[2R_m \int_{r_i}^{r} u \, dr\right] + u(1-u^2)}{r\left[4u^2 - 1\right]} \equiv \frac{F}{G} \tag{120}$$

Since we wish to start integration of Eq. (120) at the sonic point, it might appear that the unknown integral in the numerator might be

troublesome. Fortunately, this is not the case because the regularity condition requires the product of β and the exponential factor to be a known constant at the sonic point. Thus, it is possible to integrate without knowing the value of B_θ at the sonic point. B_θ is calculated from Eq. (118) after u is found. The singularity condition is $u_c = \frac{1}{2}$ and the regularity condition leads to

$$\beta = \frac{3}{5} \exp\left[2R_m \int_{r_c}^{r_i} u \, dr\right] \tag{121}$$

so that Eq. (120) becomes

$$\frac{du}{dr} = \frac{-\left(1 + 3 \exp\left[2R_m \int_{r_c}^{r} u \, dr\right]\right)u^3 + u}{r\left(4u^2 - 1\right)} \tag{122}$$

The sonic point is now the logical point to begin numerical integration. The slope at the sonic point is given by

$$\left(\frac{du}{dr}\right)_c = \frac{-1 \pm \sqrt{1 - \frac{3}{2} R_m r_c}}{4r_c} \tag{123}$$

The slope is always negative and real if $R_m r_c \leq 2/3$. This equation is plotted in Figure 28 for several values of R_m. Through each characteristic point $(0.5, r_c)$ there can be at most two possible slopes, both of which are negative. The larger of the two slopes (in absolute value) lies in Region I. Each slope in Region II corresponds to an infinite number of solutions as in Case 5 when $E > 0$. This was expected since both slopes are negative and are also subsonic and supersonic in the

same regions.

If we limit our calculations to slopes in Region I, the solutions which pass through $r_c = 1$ appear like those in Figure 29. As R_m is increased from 0 to the maximum value of 2/3, the value of β drops from 0.6 to 0.31. All the curves choke at a limit circle whose radius decreases rapidly as $R_m \to 2/3$.

By fixing R_m and integrating backwards from each value of r_c, r_i and β are obtained. These results are plotted in Figure 30 for slopes in Region I. For $R_m = 0$, $\beta = 0.6$. As R_m increases, β can take on values less than 0.6. The maximum value of r_i decreases with an increase in R_m.

The line $r_i = 3.5$ intersects the curve $R_m = 0.5$ in points A and B. These points also appear in Figure 28 in Region I. Note that point A does not lie on the dashed line, which divides the two regions, so that a portion of the curve extends below point A in Figure 30. Points between A and B in Figure 30 have values of β which correspond to solutions which pass through the sonic velocity with slopes in Region II. Therefore, as we increase β, there is first a jump in slope from A to A' in Figure 28, followed by a path to B' along the $R_m = 0.5$ curve, which is terminated by a second jump to B. If r_i is reduced to 2.5, point D lies in Region I and all points from D to C, including C, lie in Region II. Points which do not lie under the curve $R_m = 0.5$ choke.

In Figure 31, the range of values of R_m and β which permit passage through the sonic velocity is shown for $r_i = 0.35$. The solid curve CED contains points in Region I, and the shaded area, including the dashed curve CD, contains points in Region II. Line segment AB is

the same as in Figure 30.

The solution for r_i = 0.35 is shown in Figure 32. As β is reduced to the value 0.41 all the solutions choke. For β = 0.41, we have point B in Figures 30 and 31 and $\left(\dfrac{du}{dr}\right)_c$ is in Region I of Figure 28. As β is decreased the slope jumps to Region II from B' to A', and then back to Region I for point A. For values of β < 0.31 which corresponds to point A the solutions again choke. An infinite number of solutions pass through the sonic velocity in the range $0.31 \leq \beta \leq 0.41$.

If R_m = 0, this region shrinks into point D in Figure 31 and β = 0.6. The solution is shown in Figure 33. A comparison can be made with Figure 3 where the stagnation boundary condition was used instead of r_i = const.

VIII. CASE 6

Case A treats the limiting case $R_m = 0$, $N \neq 0$, in which the magnetic field interacts with the flow, but is not itself changed by the flow. For non-zero values of R_m and N both the flow and magnetic fields mutually interact. This case is concerned with the other limiting case when $N = 0$, $R_m \neq 0$. In this case, the flow distorts the magnetic field but is not itself changed by the interaction.

Assuming $\frac{\partial}{\partial z} = 0$, Eqs. (42)-(48) reduce to

$$r\rho u \;=\; m \tag{124}$$

$$\rho u \frac{du}{dr} + \alpha \frac{dp}{dr} \;=\; 0 \tag{125}$$

$$H \;=\; 1 \tag{126}$$

$$\frac{dB}{dr} + \frac{B}{r} \;=\; R_m(E + uB) \tag{127}$$

The first three equations are the ordinary gasdynamic equations which integrate to yield

$$r \;=\; \frac{m}{u(1-u^2)^{3/2}} \tag{128}$$

This is the source flow which corresponds to the $\beta = 0$ curve in Figure 3.

Equation (127) can be placed in the form

$$B \;=\; \frac{ER_m \int_{u_c}^{u} r \,\frac{dr}{du}\, \exp\!\left[-R_m \int_{r_c}^{r} u\,dr\right] du + B_c r_c}{r \,\exp\!\left[-R_m \int_{r_c}^{r} u\,dr\right]} \tag{129}$$

where r_c is given by Eq. (128) with $u_c = 0.5$. Substitution of Eq. (128) into Eq. (129) yields

$$B = \frac{ER_m \int_{1/2}^{u} f(u)g(u,mR_m)du + 1}{\frac{r}{m} g(u,mR_m)} \qquad (130)$$

where

$$
\left.
\begin{aligned}
f(u) &\equiv \frac{4u^2-1}{u^3(1-u^2)^4} \\[2em]
g(u,mR_m) &= \left[(2+\sqrt{3})\left(\frac{u}{1+\sqrt{1-u^2}}\right)\right]^{mR_m} \exp\left[-mR_m\left(\frac{u^2}{(1-u^2)^{3/2}} - \frac{2\sqrt{3}}{9}\right)\right]
\end{aligned}
\right\} \qquad (131)
$$

In Eq. (130) the boundary condition $B_c r_c = m$ has been applied.

The results of numerical integration of Eq. (130) are plotted in Figures (34) - (37). For a subsonic source with $E = 0$, as $r/m \to \infty$, $B \to 0$ when $mR_m < 1$, $B \to 0.366$ when $mR_m = 1$, and $B \to \infty$ when $mR_m > 1$. These results are shown in Figure (34). If E is increased to one, $B \to 0$ when $mR_m = 0$, and $B \to$ const. when $0 < mR_m \leq 1$. When $mR_m > 1$, $B \to \infty$. These results appear in Figure (35).

For a supersonic source the magnetic field $B \to \infty$ with r/m when $mR_m > 0$ and $B \to 0$ when $mR_m = 0$. The distribution of B is shown in Figure 36 for $E = 0$ and in Figure 37 for $E = 1.0$.

The limiting values of B for large r/m are summarized in Table IV.

TABLE IV

	SUPERSONIC SOURCE	SUBSONIC SOURCE
$E = 0$	$B \to \infty$	$B \to 0 \qquad 0 \leq mR_m < 1$ $B \to 0.366 \qquad mR_m = 1$ $B \to \infty \qquad mR_m > 1$
$E = 1.0$	$B \to \infty$	$B \to 0 \qquad mR_m = 0$ $B \to \text{const}, \; 0 < mR_m \leq 1$ $B \to \infty \qquad mR_m > 1$

IX. CONCLUSIONS

Solutions have been obtained for magnetogasdynamic source flow with crossed electric and magnetic fields. The solutions have been restricted to those which pass through the sonic velocity.

For the case where $R_m = K = 0$, the sonic circle can be placed at any radius. If $E > 0$, an infinite number of solutions decelerate through $M = 1$ with the same velocity gradient. There is one other solution which also decelerates through $M = 1$ with a different gradient in velocity. If $E < 0$, four different solutions can pass through sonic velocity at any given location of the sonic circle. Three of these are accelerating flows.

The effect of non-zero magnetic Reynolds number was found for source flow with $E = 0$. When $R_m = 0$ there is one solution which passes through $M = 1$ when $\beta = 0.6$. When $R_m > 0$ there is a range of β in which solutions are possible. If R_m is increased beyond a certain limit, no solutions are possible.

The displacement of the magnetic field by ordinary gasdynamic source flow was obtained for the limiting case when $\beta = 0$, $R_m \neq 0$. For a supersonic source the magnetic field always increases to infinity with the radius for finite R_m. For a subsonic source this occurs only if $mR_m > 1$. For other values of mR_m the field approaches a constant value or zero.

These results indicate many possibilities exist for the passage through the sonic velocity without the need of a throat in magnetogasdynamics.

APPENDIX A

ACCELERATION THROUGH A CONSTANT AREA CHANNEL

This section deals with the flow through a constant area channel with crossed electric and magnetic fields. The configuration is shown in Figure A-1.

The governing equations in dimensionless form are

$$\rho u \; = \; m \tag{A-1}$$

$$\rho u \frac{du}{dx} + \alpha \frac{dp}{dx} \; = \; -N(E+u) \tag{A-2}$$

$$\rho u \left[\frac{dT}{dx} + 2u \frac{du}{dx} \right] \; = \; 2NE(E+u) \tag{A-3}$$

$$p \; = \; \rho T$$

Eliminating the pressure and density yields

$$\frac{dU}{dx} \; = \; \frac{-\beta U(1-U)(2-5U)}{3U^2 - t} \; \equiv \; \frac{F}{G} \tag{A-5}$$

$$\frac{dt}{dx} \; = \; 2\beta(1-U) - 2U \frac{dU}{dx} \tag{A-6}$$

where

$$U \; = \; -\frac{u}{E} \qquad t \; = \; \frac{T}{E^2} \qquad \gamma \; = \; 5/3 \tag{A-7}$$

The singularity condition G = 0 leads to

$$t_c \; = \; 3U_c^2 \tag{A-8}$$

and the regularity condition F = 0 leads to

$$U_c \; = \; 0, \quad U_c \; = \; 1, \quad U_c \; = \; 0.4 \tag{A.9}$$

The two slopes at a characteristic point are

$$
\left.\begin{array}{l}
\left(\dfrac{dU}{dx}\right)_c = \dfrac{\beta(12 - 15U_c)}{8} \\[4mm]
\left(\dfrac{dU}{dx}\right)_c = 0
\end{array}\right\}
\qquad\text{(A.10)}
$$

The properties at the three characteristic points are summarized in Table A-I.

<div align="center">TABLE A-I</div>

u_c	t_c		$\left(\dfrac{dU}{dx}\right)_c$		$\left(\dfrac{dt}{dx}\right)_c$
0	0	0	1.5β	2β	2β
0.4	0.48	0	0.75β	1.2β	0.6β
1.0	3.0	0	-0.375β	0	0.75β

Since Eqs. (A-5) and (A-6) do not contain x, we can divide the two equations to eliminate dx to obtain

$$
\frac{dU}{dt} = \frac{U(5U - 2)}{-10U^3 + 10U^2 - 2t} \equiv \frac{P}{Q}
\qquad\text{(A.11)}
$$

This equation in the phase plane is independent of β. Two characteristic points exist and the properties of the solutions through these points are summarized in Table A-II.

<div align="center">TABLE A-II</div>

u_c	t_c		$\left(\dfrac{dU}{dt}\right)_c$
0	0	0	0.75
0.4	0.48	0	1.25

The solutions in the phase plane are shown in Figure A-2. The projection of the solutions on the U-x and t-x planes are shown in Figures A-3 and A-4, respectively.

Solution Ia accelerates from zero temperature and velocity through the sonic velocity to $M = \sqrt{5}$ at $x = \infty$. The temperature reaches a maximum at $x = 0.9$ where $U = 0.9$. Energy is always added to the flow, but the rate of addition diminishes with x. In solution Ib, the velocity is constant and the temperature increases linearly with x, so that the initially supersonic flow becomes subsonic. Energy is added to the flow at a constant rate.

Energy is first extracted from the flow when it is supersonic and then added when it becomes subsonic in solution IIa. The flow begins at $U = 2.34$ with zero temperature and decelerates to $U = 0.4$ and infinite temperature. Solution IIb is a constant Mach number flow at the sonic velocity.

A closed form solution corresponding to Ia and Ib appears in Reference 4. Solutions Ia and IIa were discussed in Reference 5, but calculations were not made.

REFERENCES

1. Hains, F. D., "The Magnetogasdynamic Source," Boeing Document D1-82-0166, May 1962.

2. Sherman, A., "Theoretical Performance of a Crossed Field MHD Accelerator," A.R.S. Journal, Vol. 32, No. 3, pp. 414-420, March 1962.

3. Podolsky, B. and Borman, G., "The Electromagnetic Acceleration of a Continuously Flowing Plasma," Plasma Acceleration, Stanford University Press, 1960.

4. Oates, Gordon C., "Constant-Electric-Field and Constant-Magnetic-Field Magnetogasdynamic Channel Flow," Readers' Forum, Journal of the Aerospace Sciences, Vol. 29, No. 2, pp. 231-232, February 1962.

5. Resler Jr., E. L. and Sears, W. R., "Magneto-Gasdynamic Channel Flow," ZAMP, Vol. IXb, pp. 509-518, 1958.

ACKNOWLEDGEMENT

The author wishes to thank G. J. Thomas for carrying out the computer calculations.
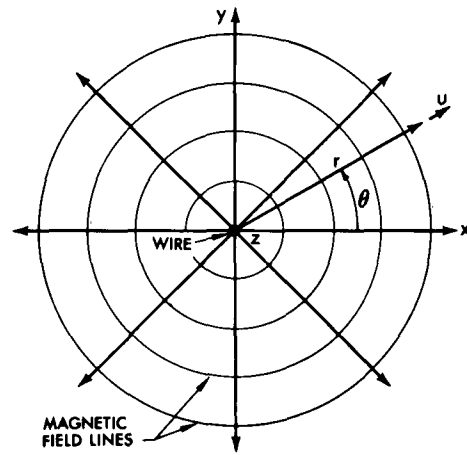
Fig. 1.   Coordinate system and geometry of MGD source.
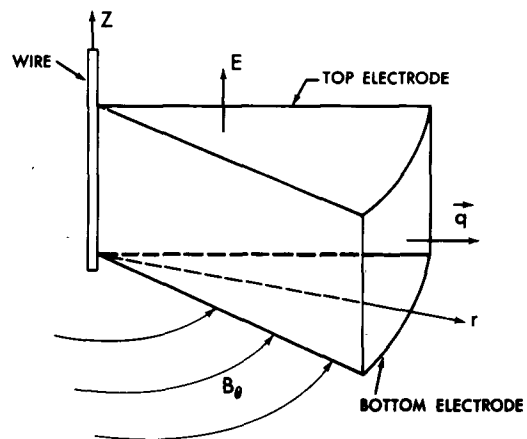
Fig. 2.   Coordinate system and geometry of diverging channel.
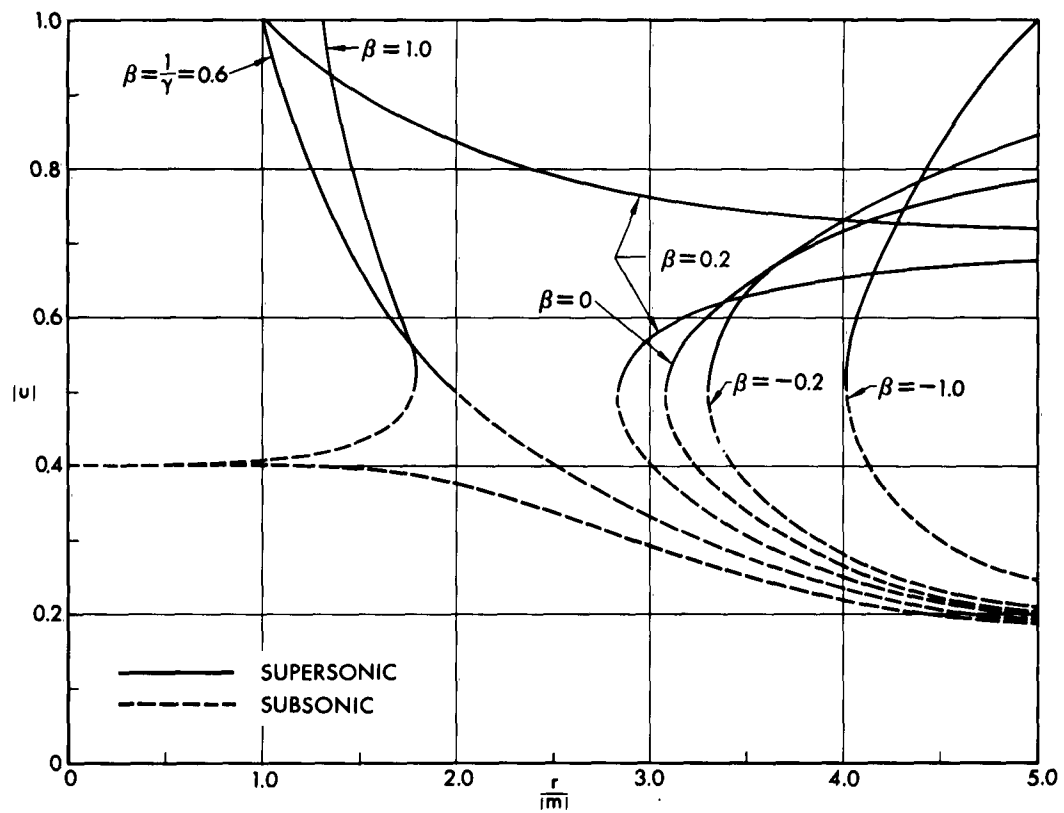
Fig. 3.   Case A.   Velocity distribution for various values of
the interaction parameter β.   Isoenergetic flow E = 0.
β > 0, source; β < 0, sink.
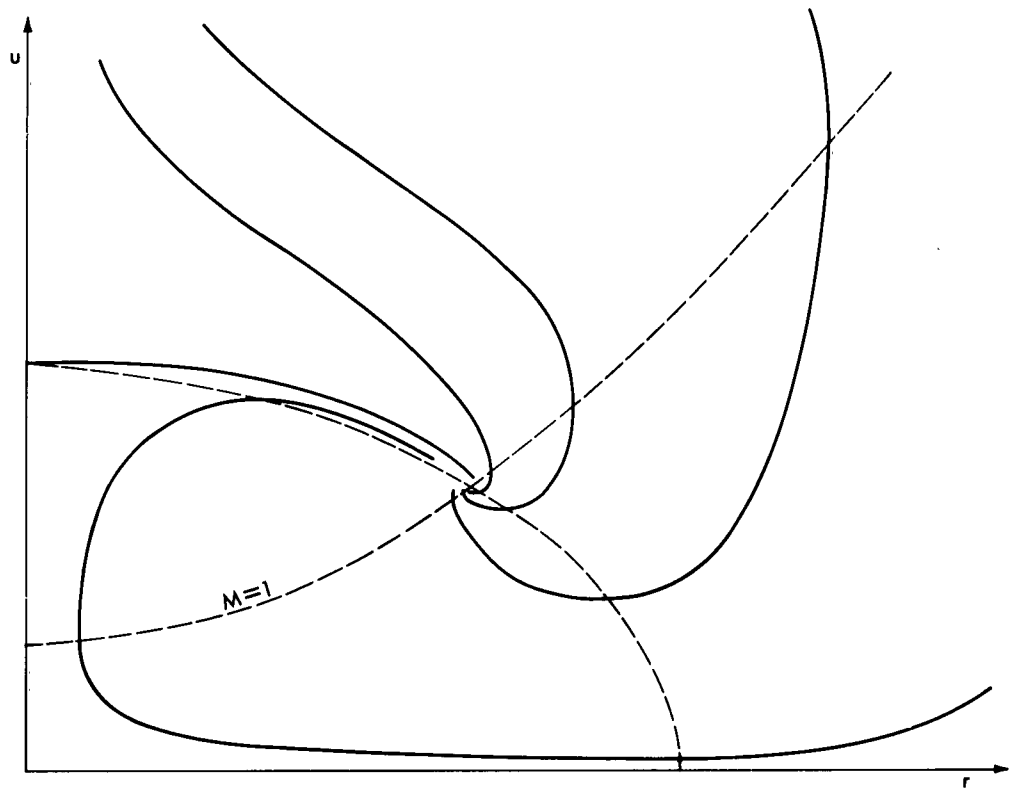
Fig. 4.   Sketch of Case B, source with $R_m = B = 0$.   E = const.
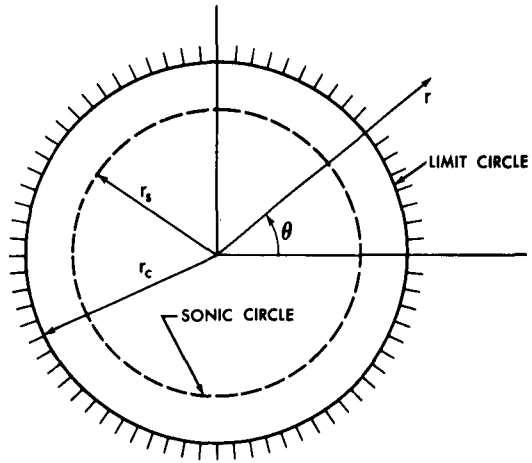
Fig. 5a.   Location of sonic circle and limit circle when solution
            is inside the limit circle.
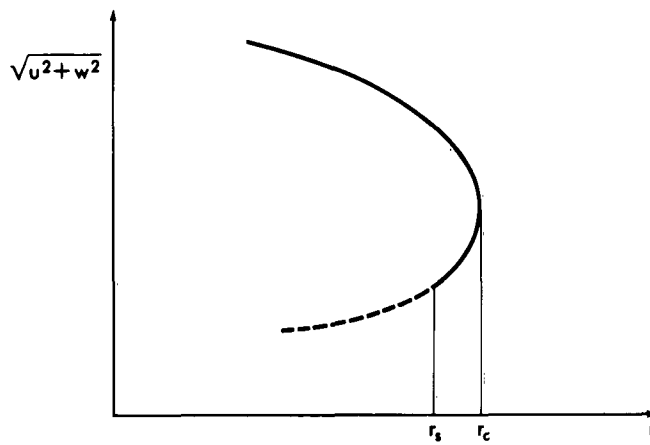
Fig. 5b.   Velocity distribution for solution inside limit circle.
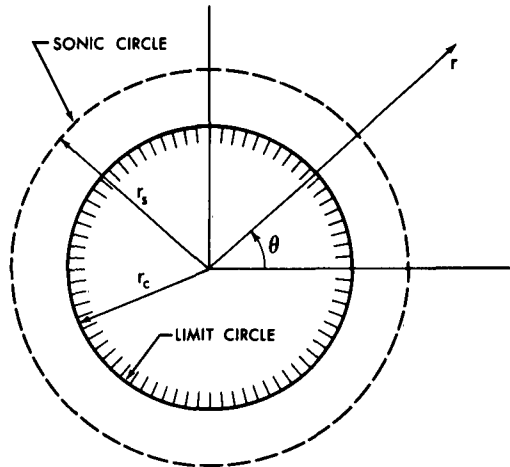
Fig. 5c.   Location of sonic circle and limit circle when solution

is outside the limit circle.
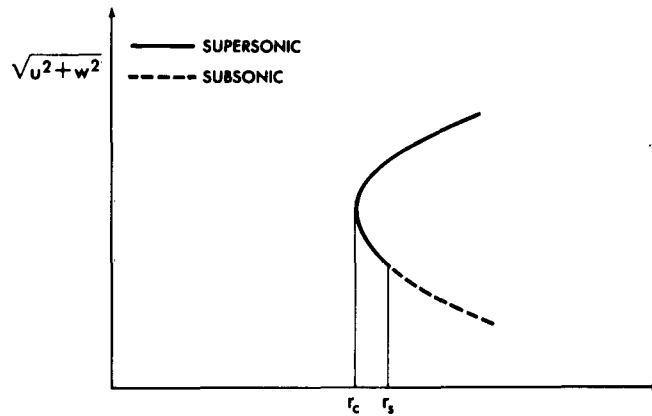
Fig. 5d.   Velocity distribution for solution outside limit circle.
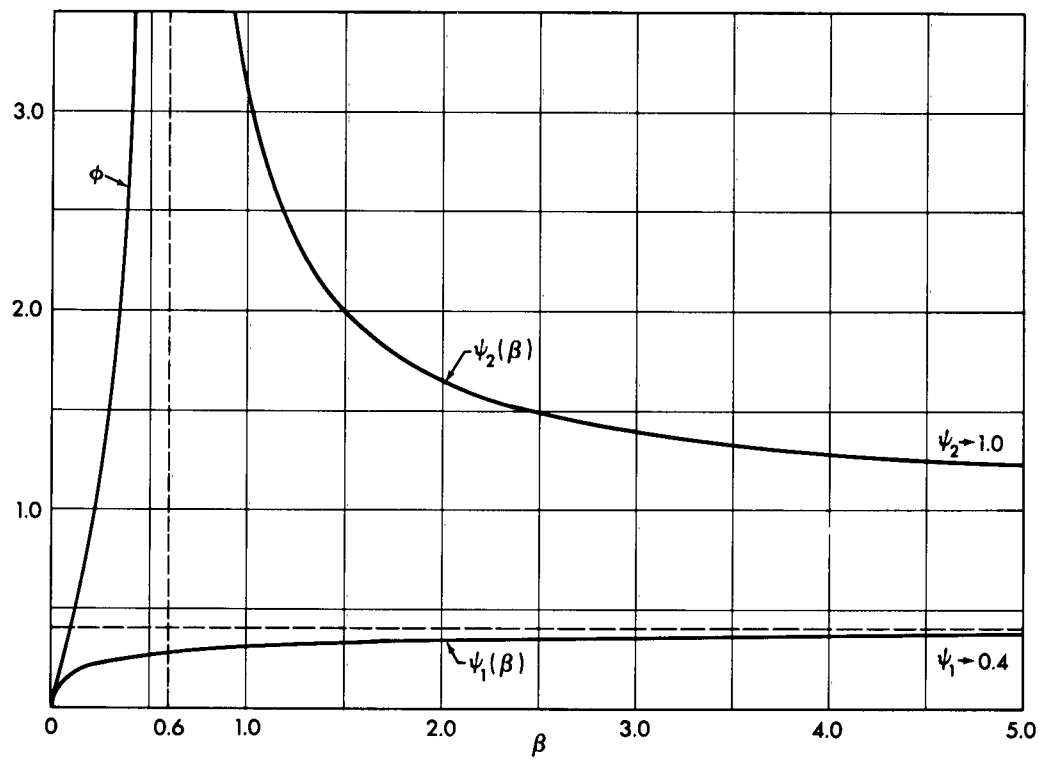
Fig. 6. Variation of ψ_1, ψ_2 and ϕ with β. Case 4, E < 0.
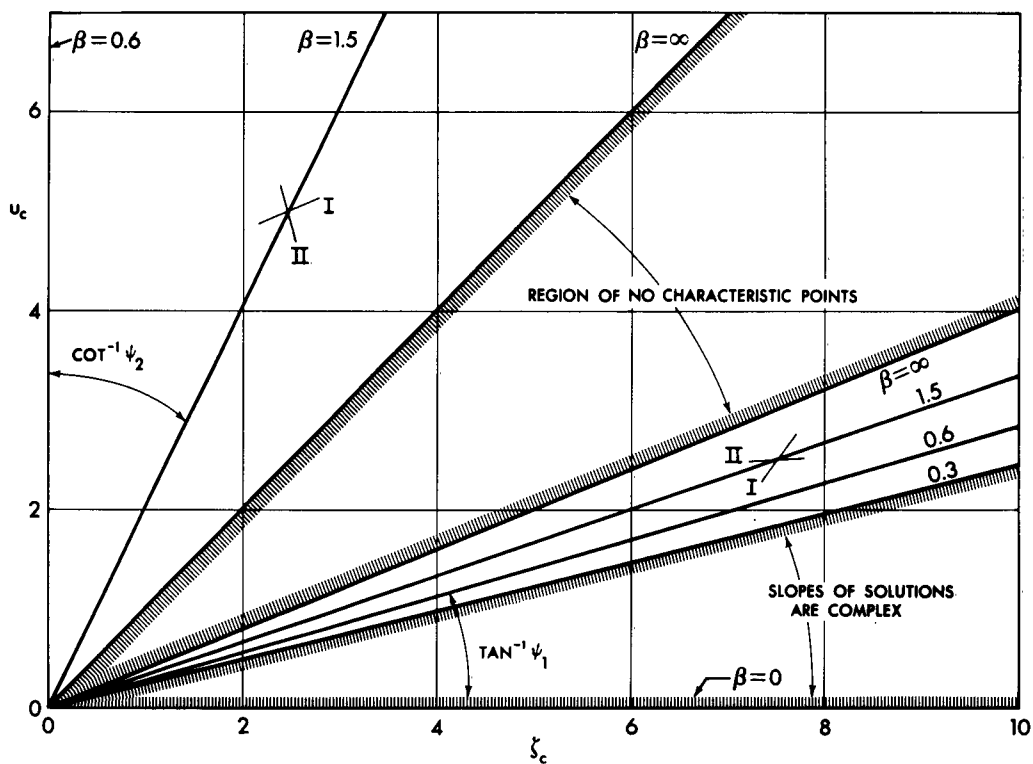
Fig. 7.   Locus of characteristic points in the u_c-ζ_c plane.
Case 4, E < 0.
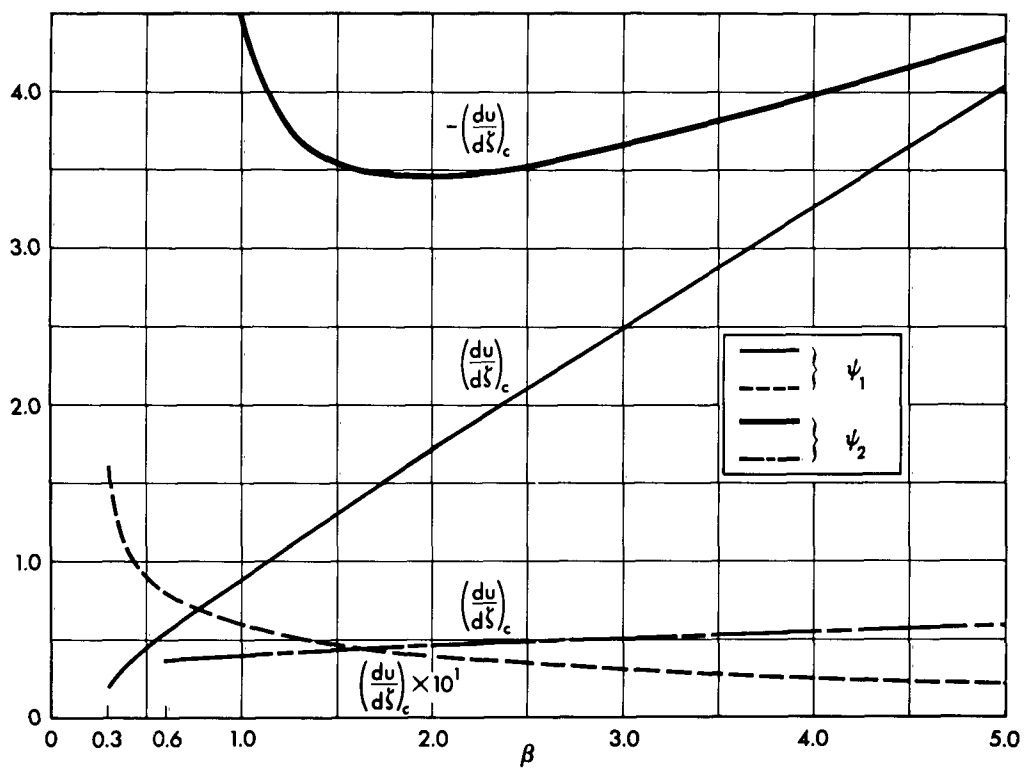
Fig. 8.   Variation of $\left(\dfrac{du}{d\zeta}\right)_c$ with β.   Case 4, $E < 0$.
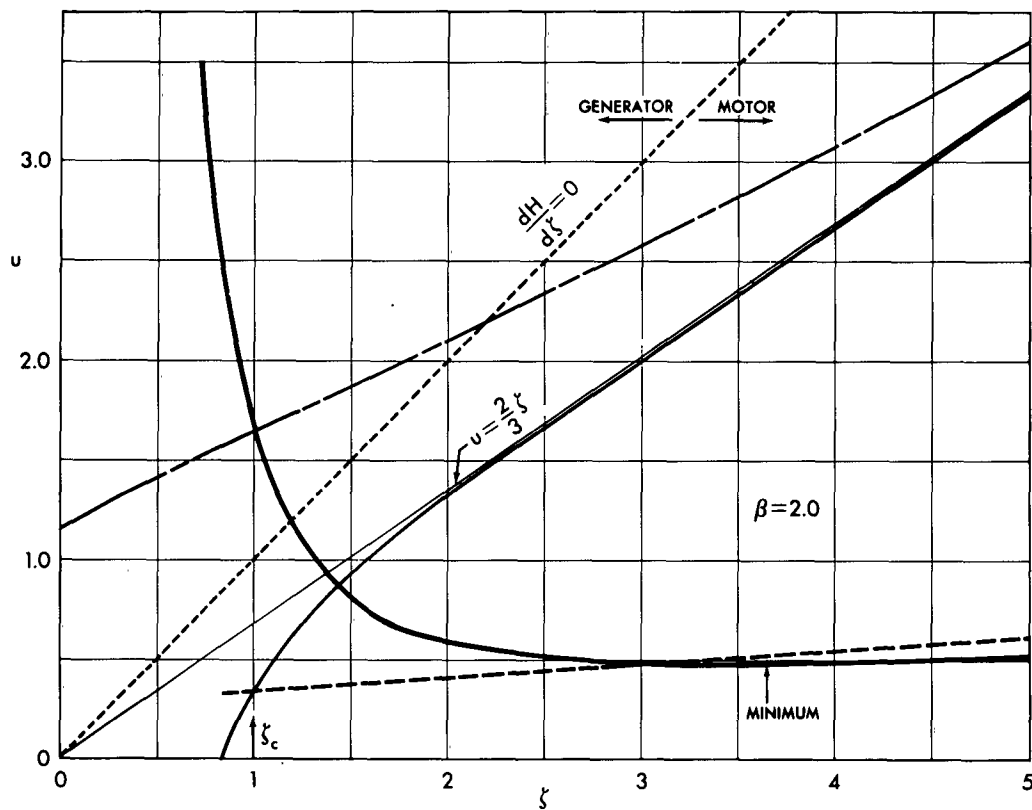
Fig. 9.   Variation of u with ζ for ζ_c = 1 and β = 2.   Case 4,

E < 0.
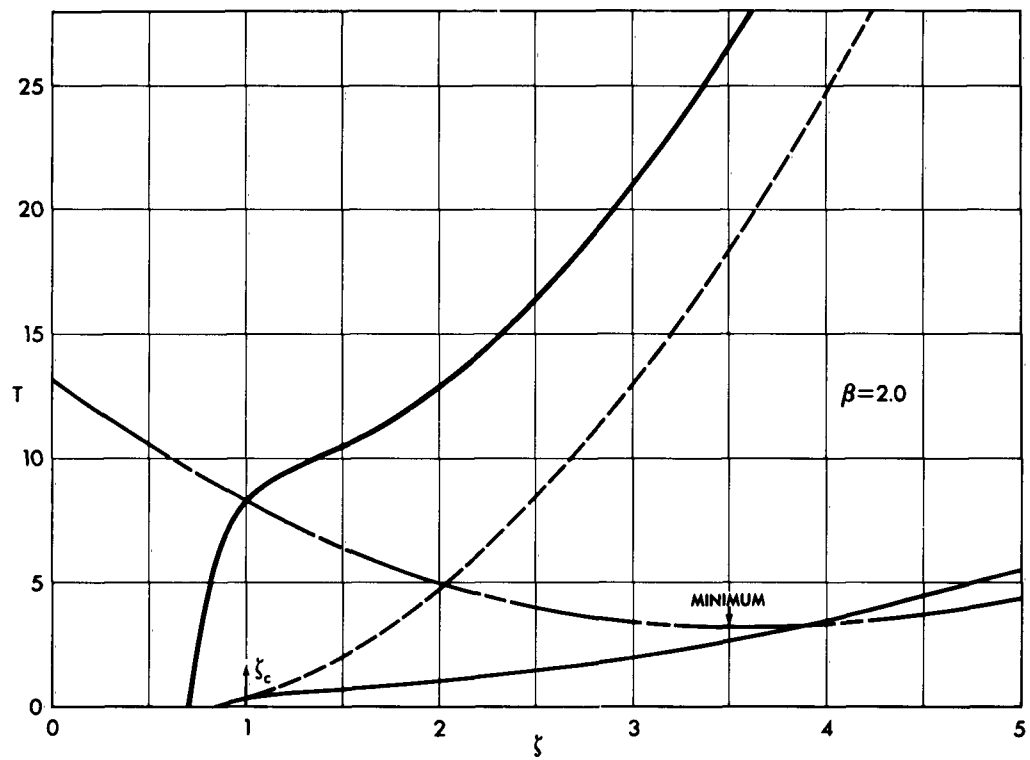
Fig. 10. Variation of T with ζ for $\zeta_c = 1$ and $\beta = 2$. Case 4, $E < 0$.
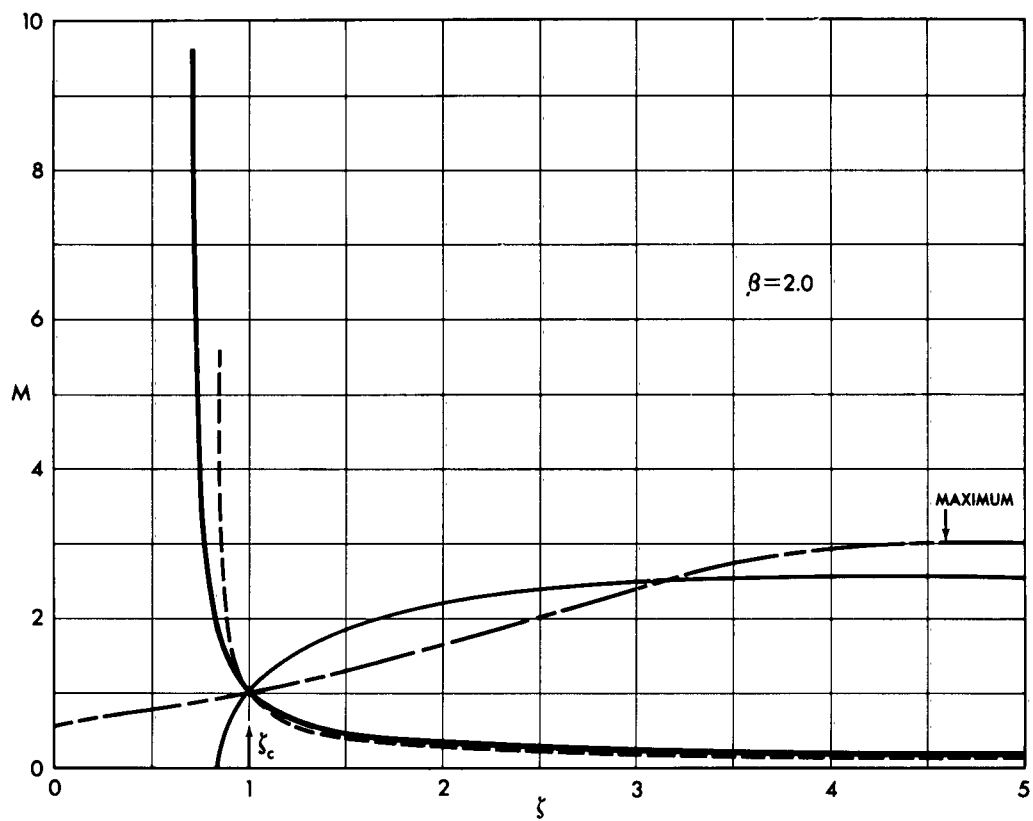
Fig. 11.   Variation of M with ζ for $\zeta_c = 1$ and $\beta = 2$. Case 4, $E < 0$.
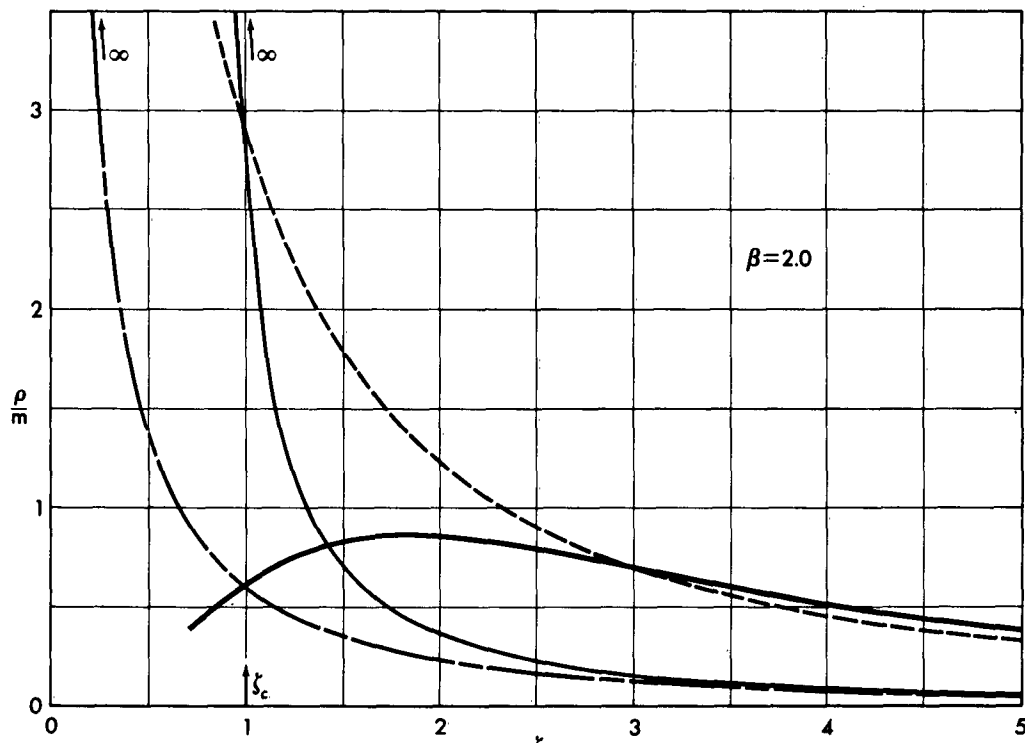
Fig. 12.   Variation of $\frac{\rho}{m}$ with ζ for $\zeta_c = 1$ and $\beta = 2$.   Case 4, $E < 0$.
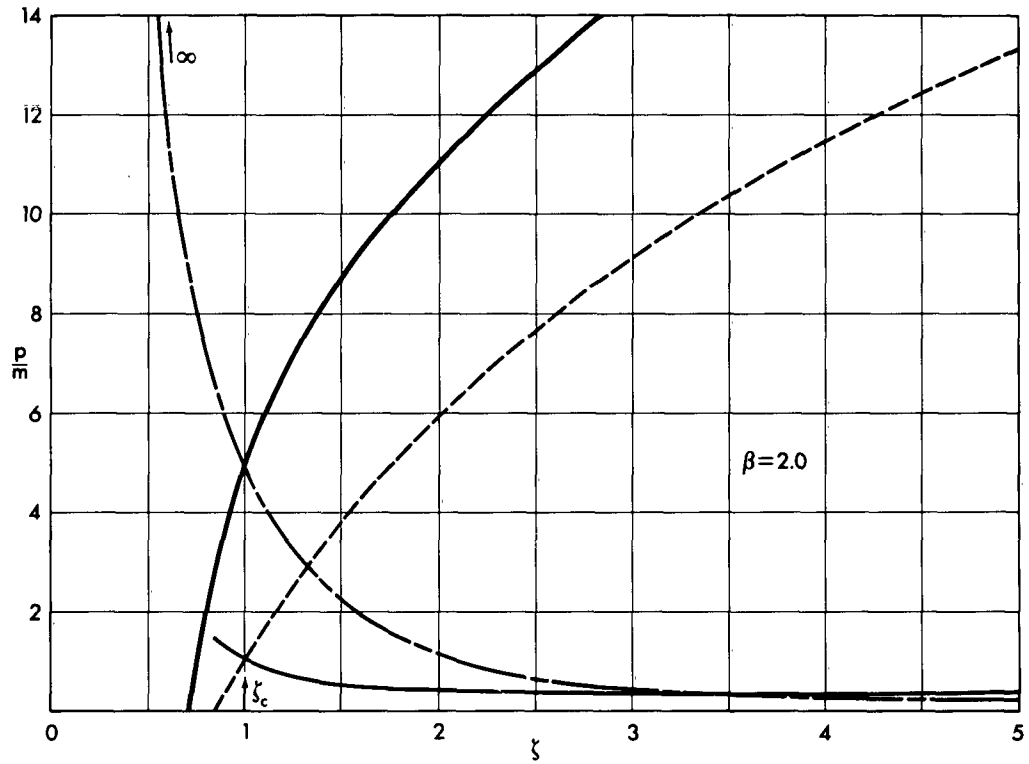
Fig. 13. Variation of $\frac{p}{m}$ with ζ for $\zeta_c = 1$ and $\beta = 2$. Case 4, $E < 0$.
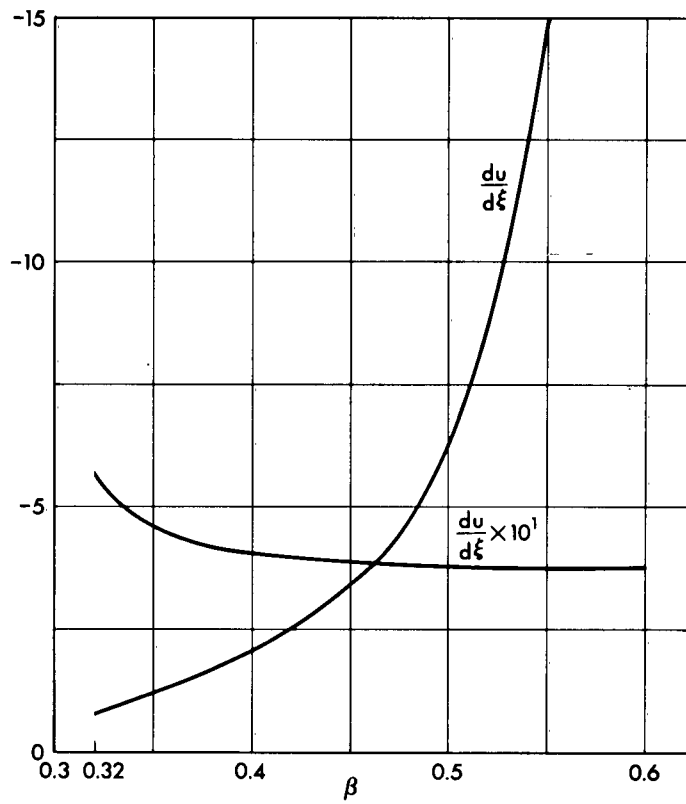
Fig. 14. Variation of $\frac{du}{d\zeta}$ with β. Case 4, $E > 0$.
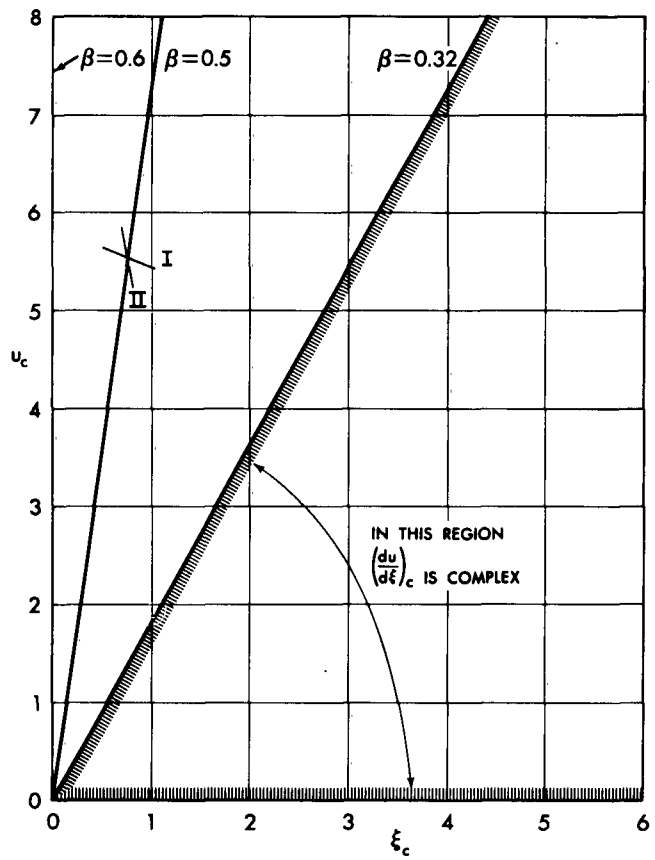
Fig. 15. Locus of characteristic points in the u_c-ζ_c plane.
Case 4, $E > 0$.
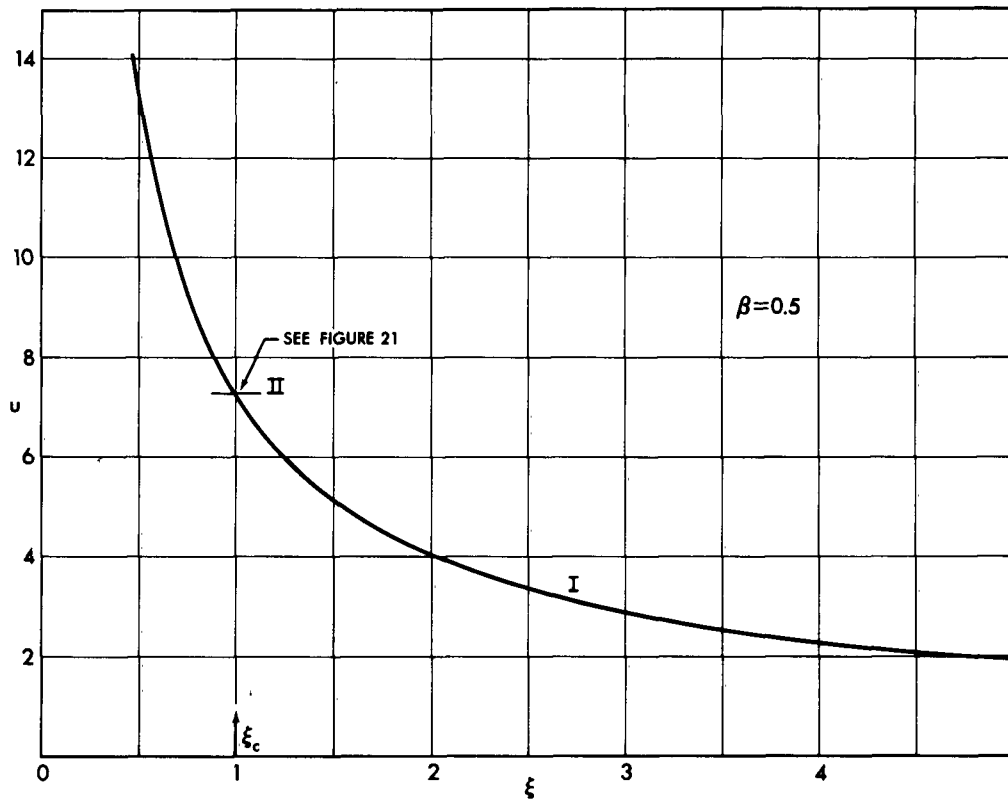
Fig. 16. Variation of u with ξ for $\xi_c = 1$ and $\beta = 0.5$. Case 4,
E > 0.
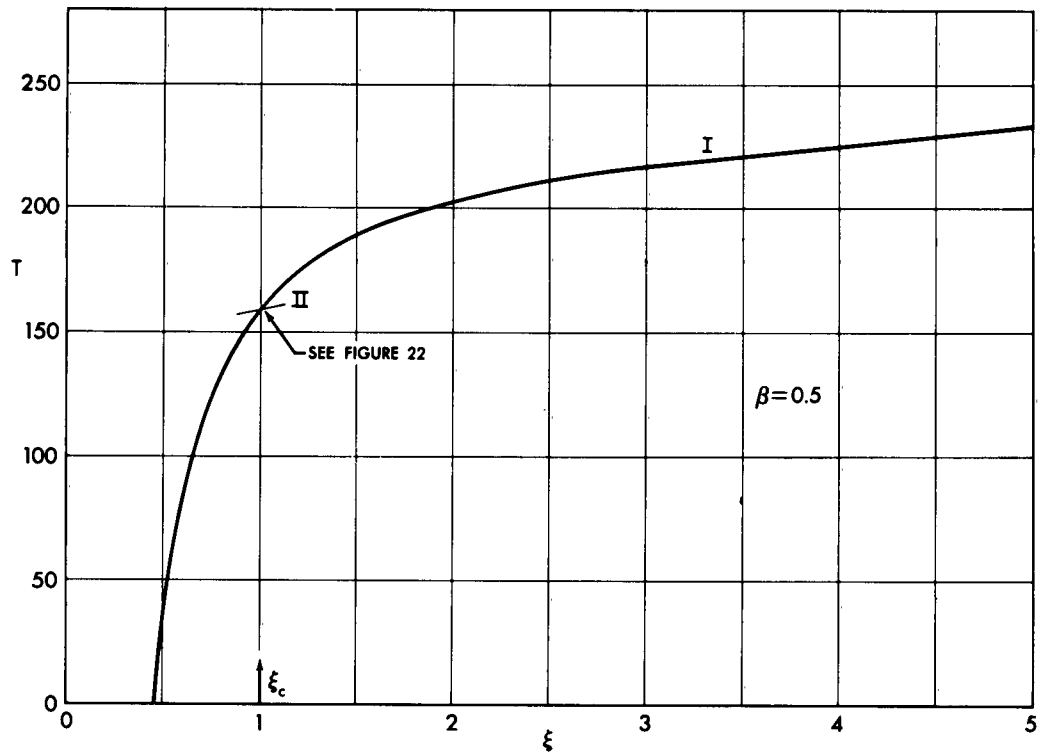
Fig. 17. Variation of T with ξ for ξ_c = 1 and β = 0.5. Case 4, E > 0.
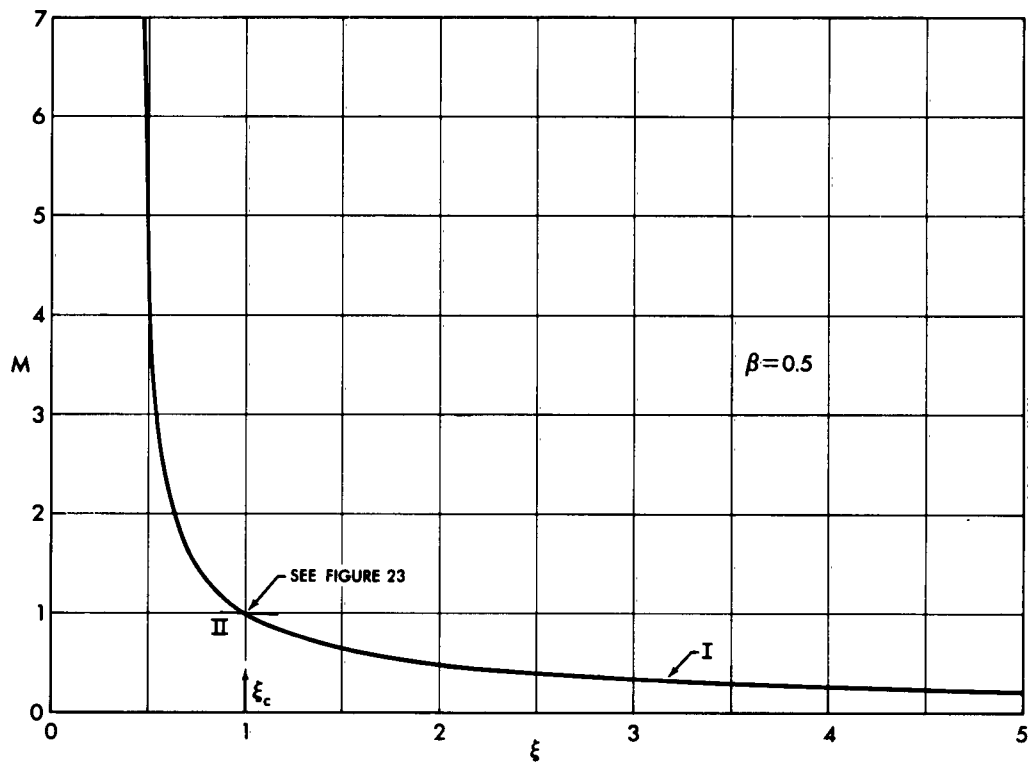
Fig. 18.   Variation of M with ξ for $\xi_c = 1$ and $\beta = 0.5$.   Case 4, $E > 0$.
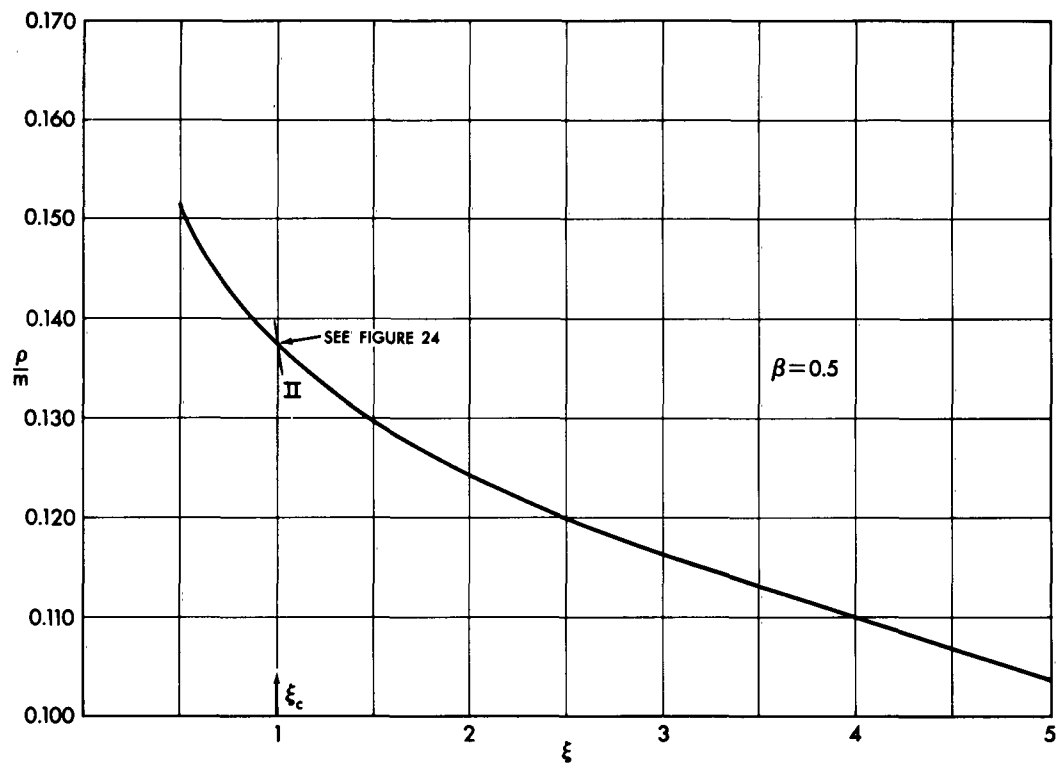
Fig. 19.   Variation of $\frac{\rho}{m}$ with ζ for $\zeta_c = 1$ and $\beta = 0.5$.   Case 4,

E > O.
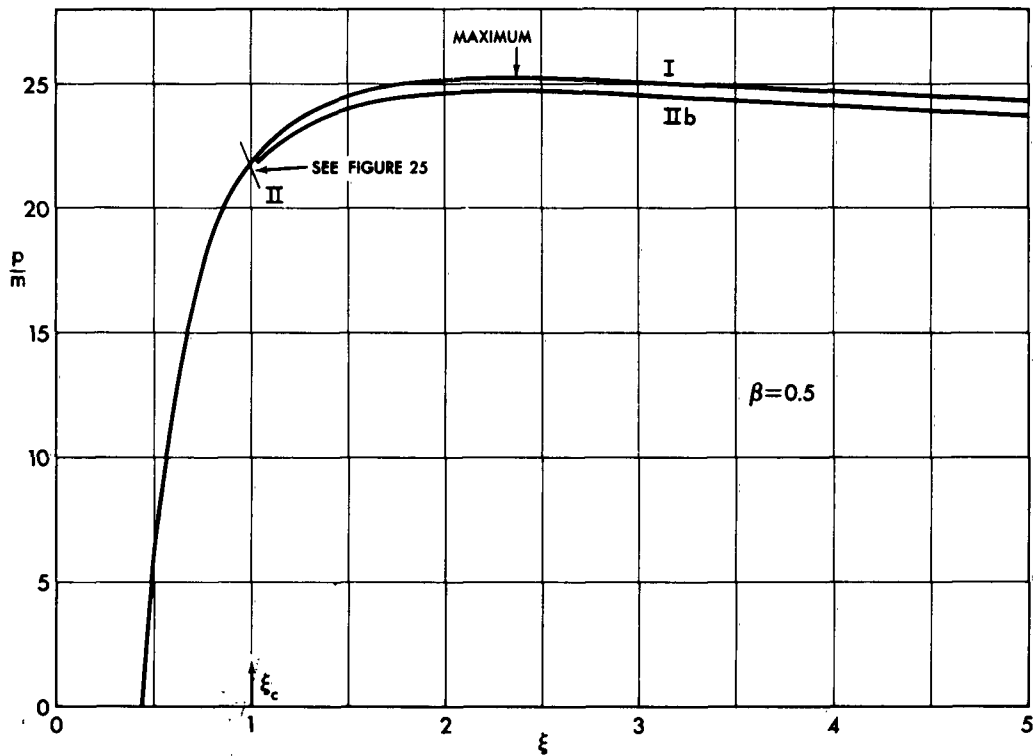
Fig. 20.   Variation of $\frac{p}{m}$ with ξ for $\xi_c = 1$ and $\beta = 0.5$.   Case 4, $E > 0$.
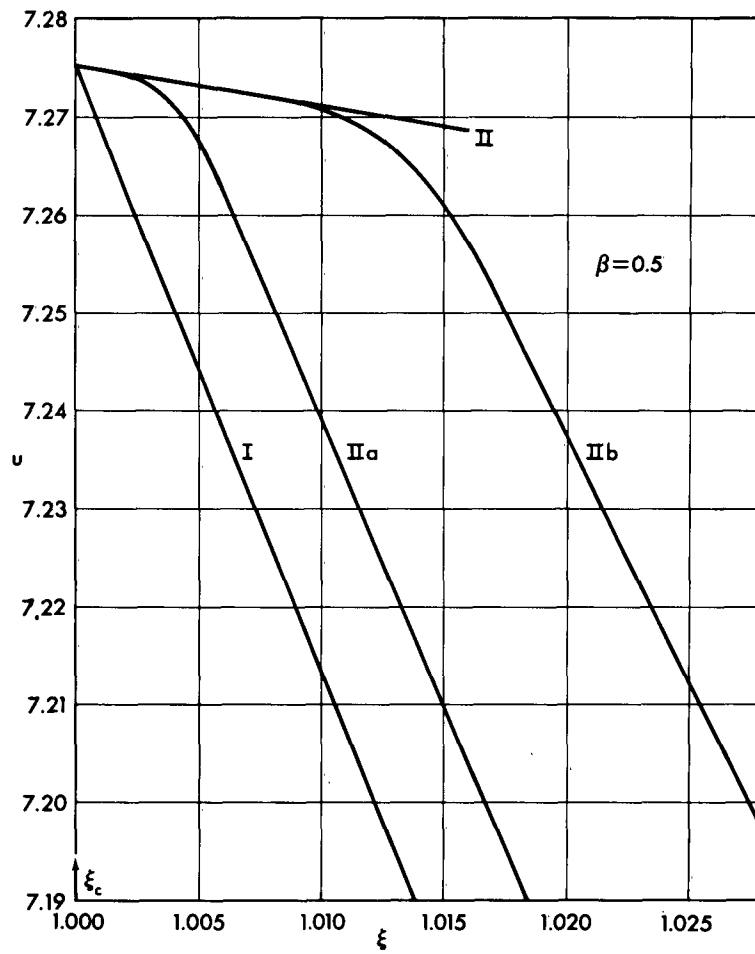
Fig. 21.   Variation of u with ζ for ζ$_c$ = 1 and β = 0.5.   Case 4,
E > 0.
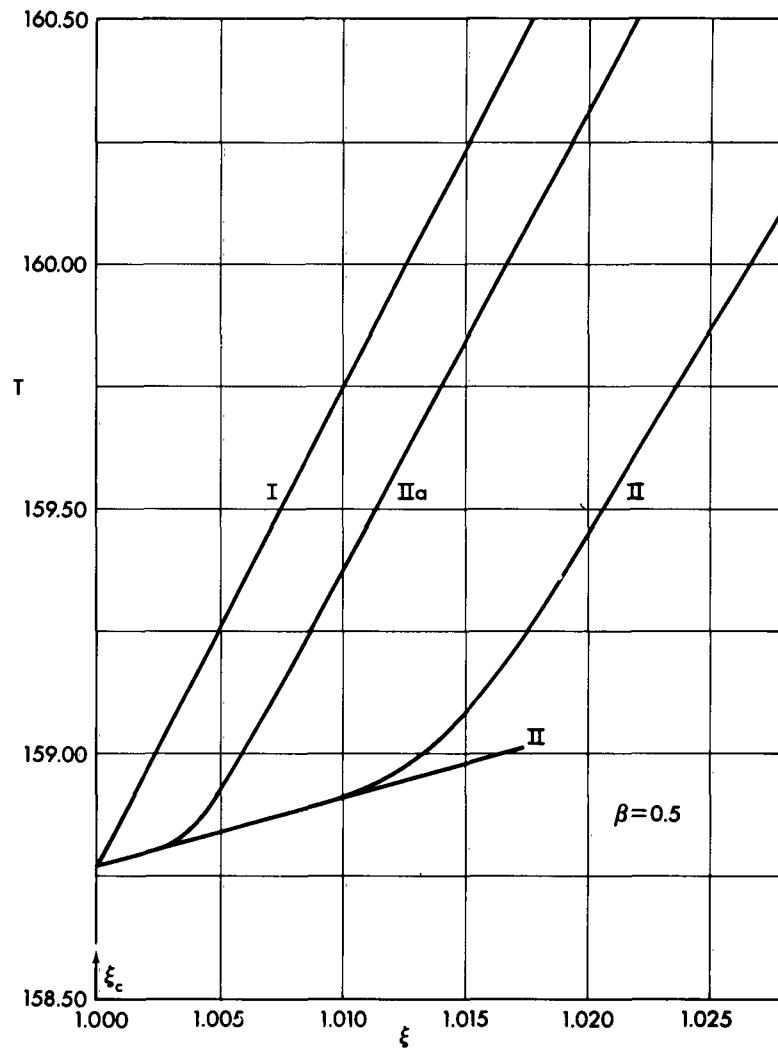
Fig. 22.   Variation of T with ζ for $\zeta_c = 1$ and $\beta = 0.5$.   Case 4,
E > 0.
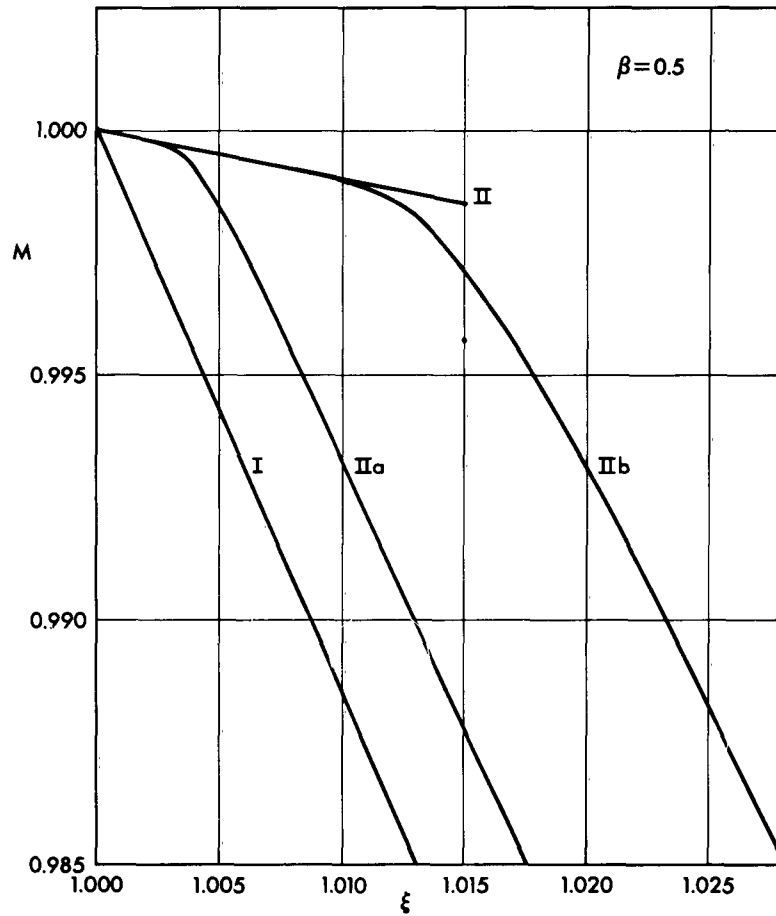
Fig. 23. Variation of M with ξ for $\zeta_c = 1$ .nd $\beta = 0.5$. Case 4, $E > 0$.
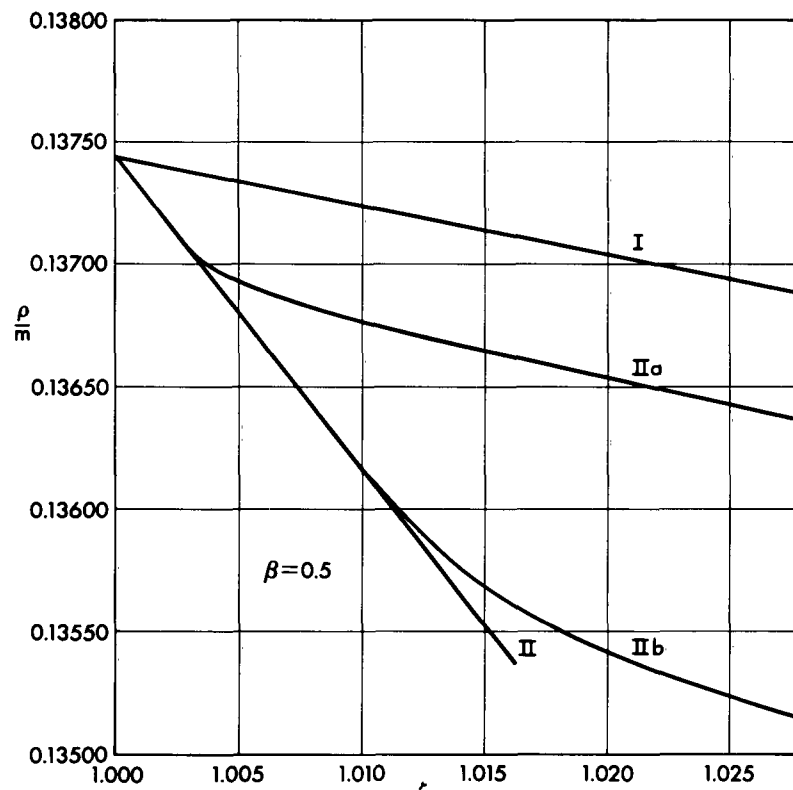
Fig. 24. Variation of $\frac{\rho}{m}$ with ζ for $\zeta_c = 1$ and $\beta = 0.5$. Case 4, $E > 0$.
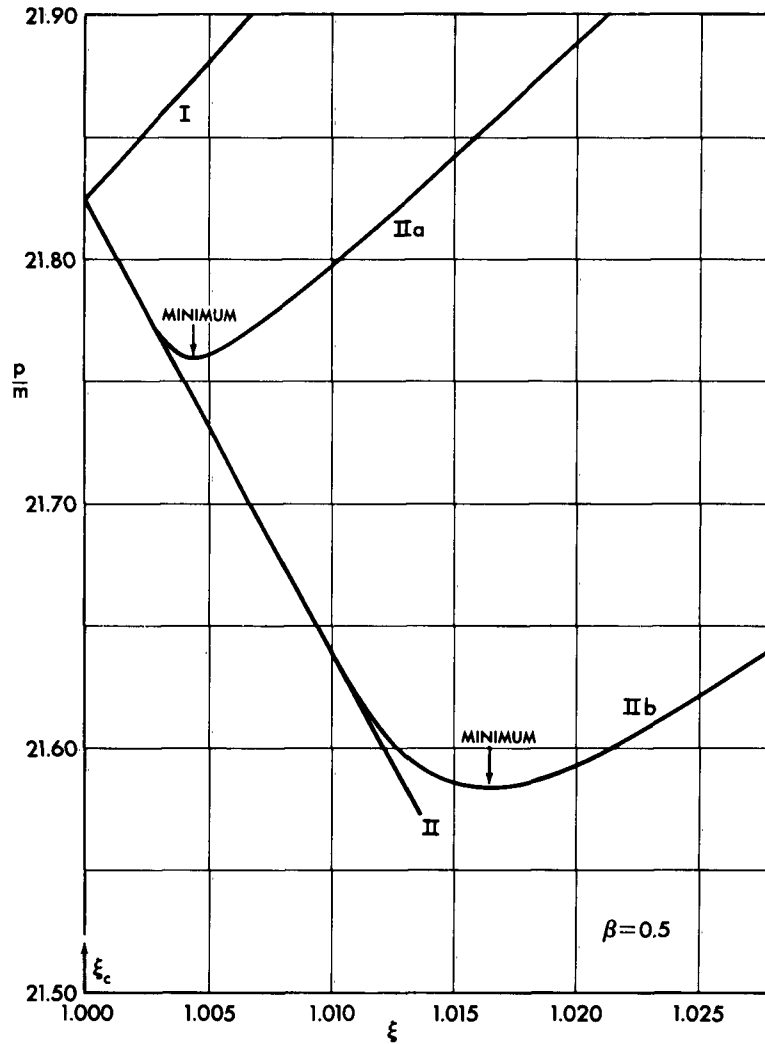
Fig. 25. Variation of $\frac{p}{m}$ with ζ for $\zeta_c = 1$ and $\beta = 0.5$. Case 4, $E > 0$.
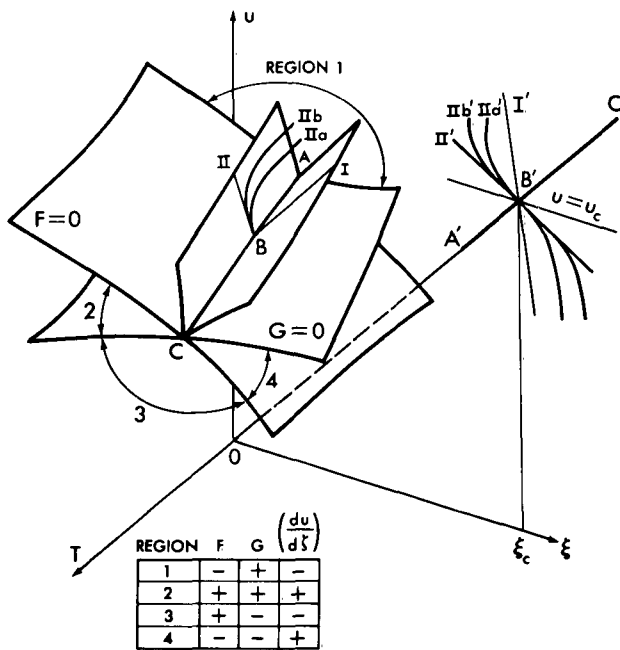
Fig. 26.   The solution in the u - T - ξ coordinate system.
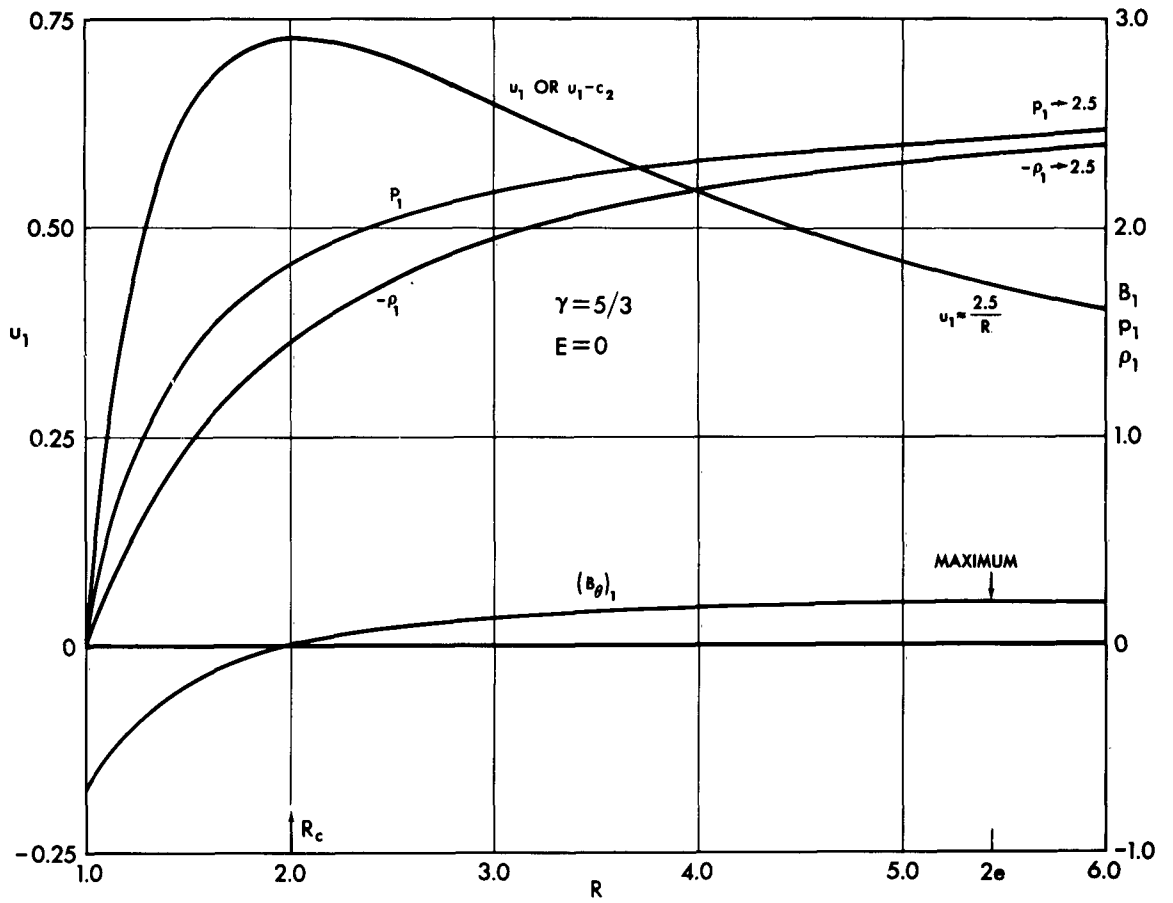
Fig. 27.   Variation of the perturbation variables with R.

Case 5.
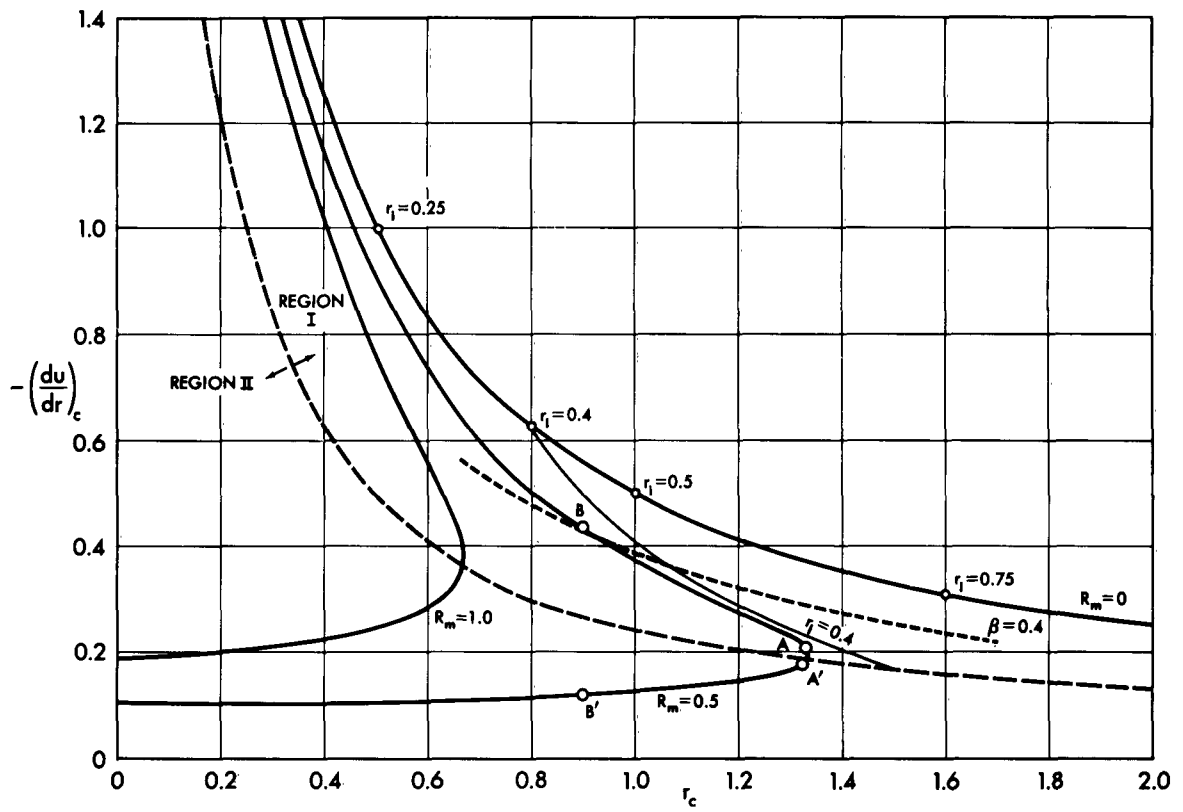
Fig. 28. Variation of $\left(\dfrac{du}{dr}\right)_c$ with r_c. Case 5.
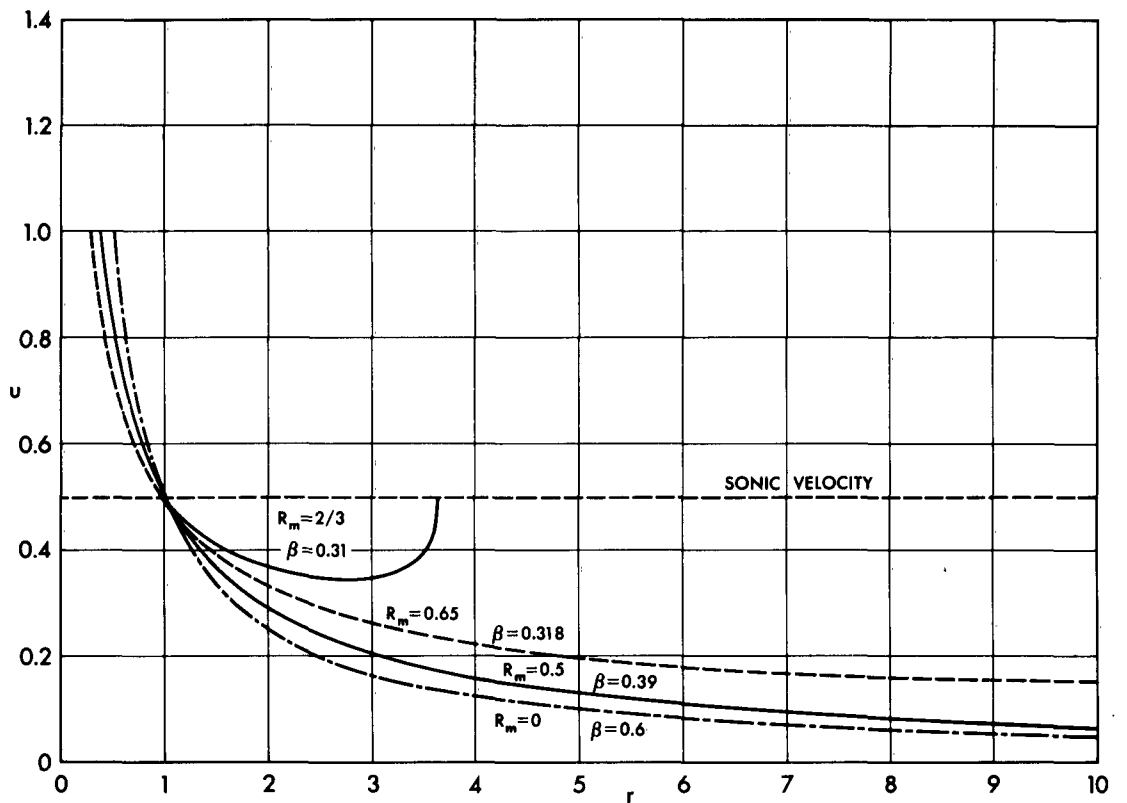
Fig. 29. Velocity distribution. $r_c = 1$ and $\left(\dfrac{du}{dr}\right)_c$ from region I of Figure 28. Case 5.
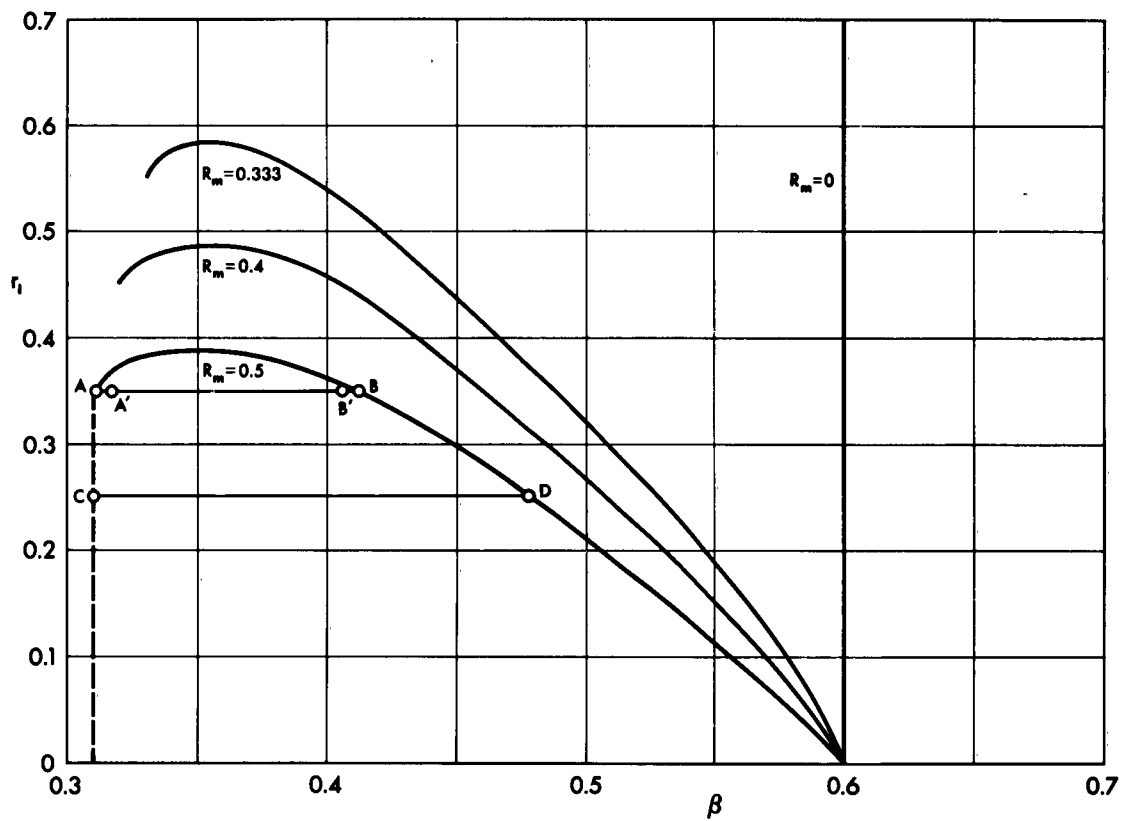
Fig. 30. Variation of r_i with β for fixed R_m. Case 5.
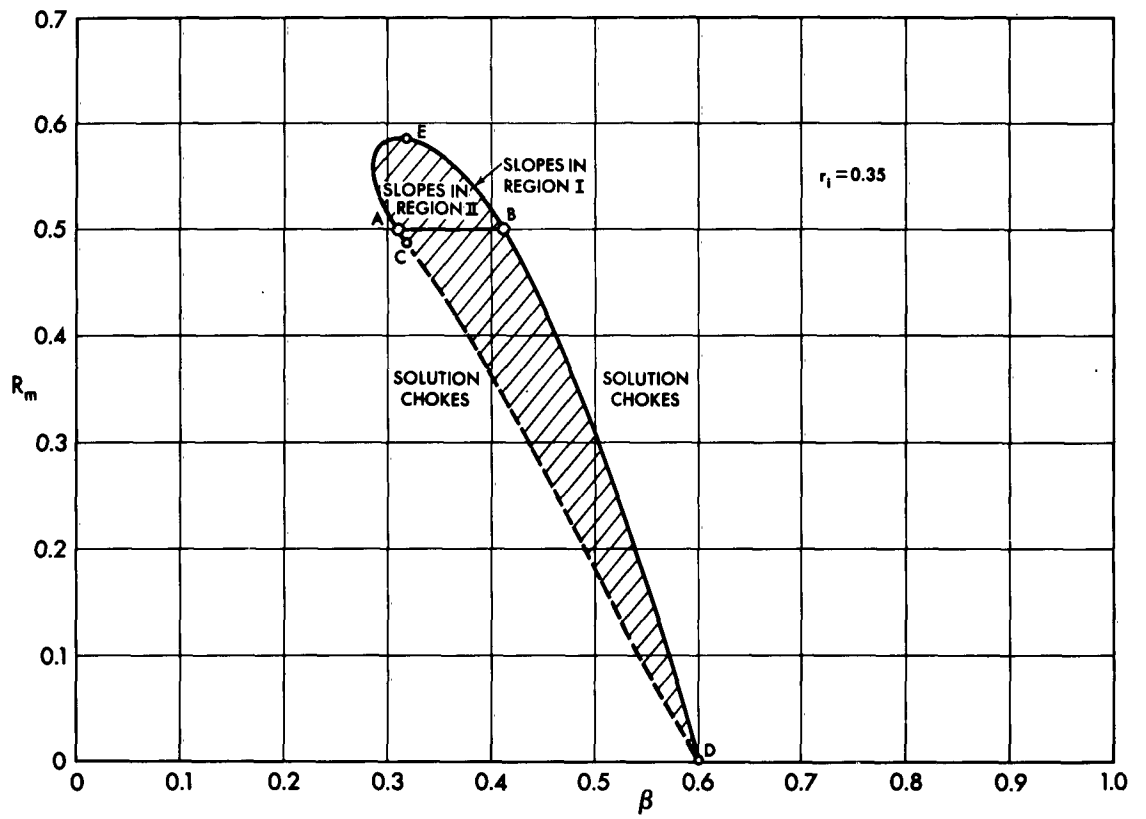
Fig. 31. R_m vs. β when $r_i = 0.35$.
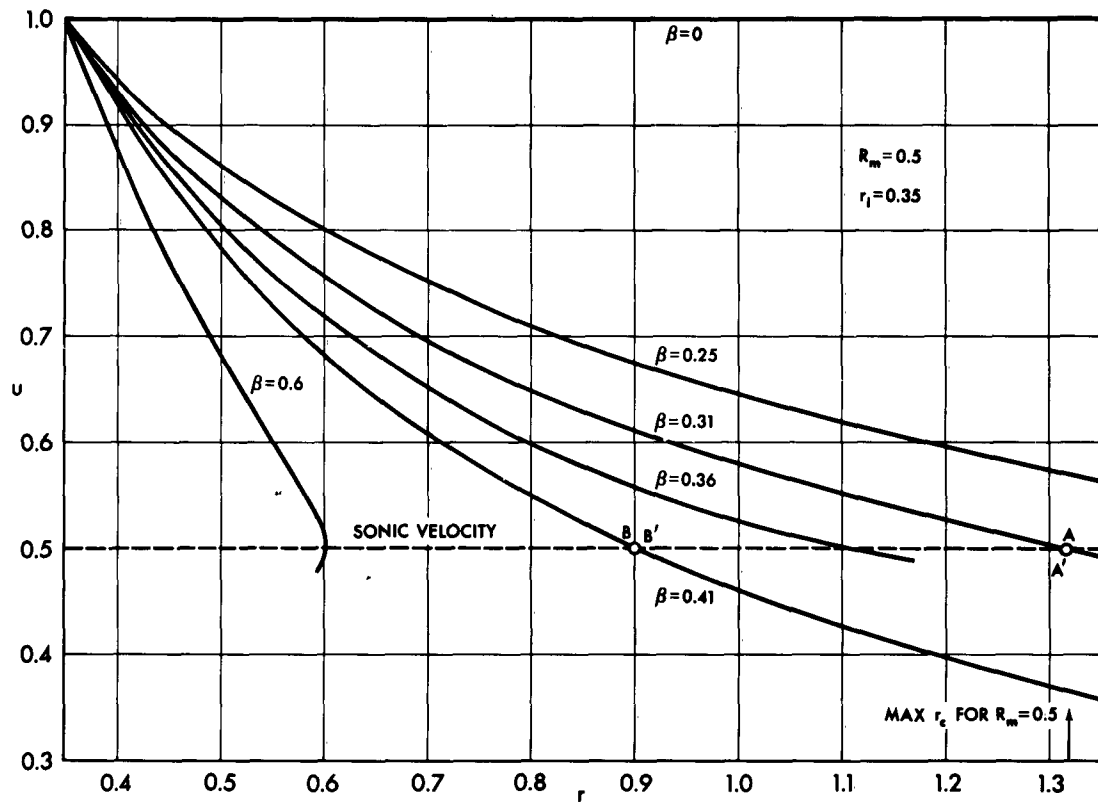
Fig. 32.   Velocity distribution for various values of β. u_i = 1.0,

r_i = 0.35, R_m = 0.5.   Case 5.
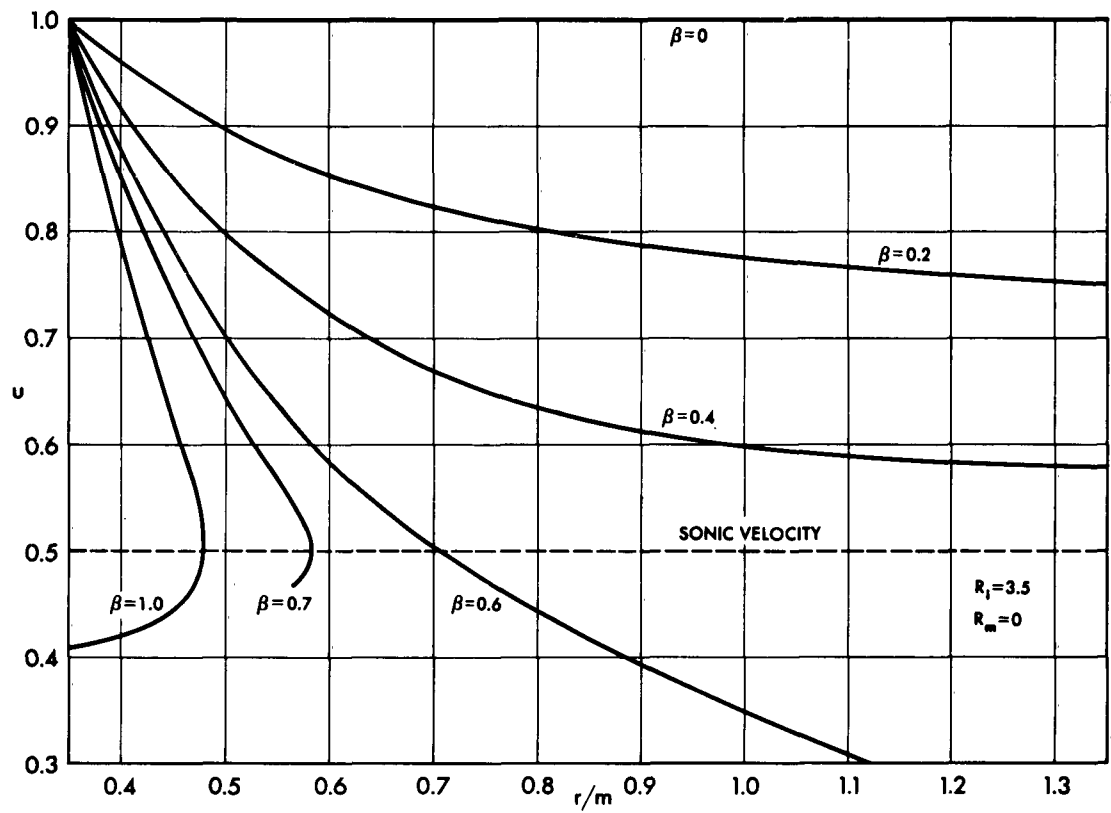
Fig. 33. Velocity distribution for various values of β. $u_i = 1$, $r_i = 0.35$, $R_m = 0$.
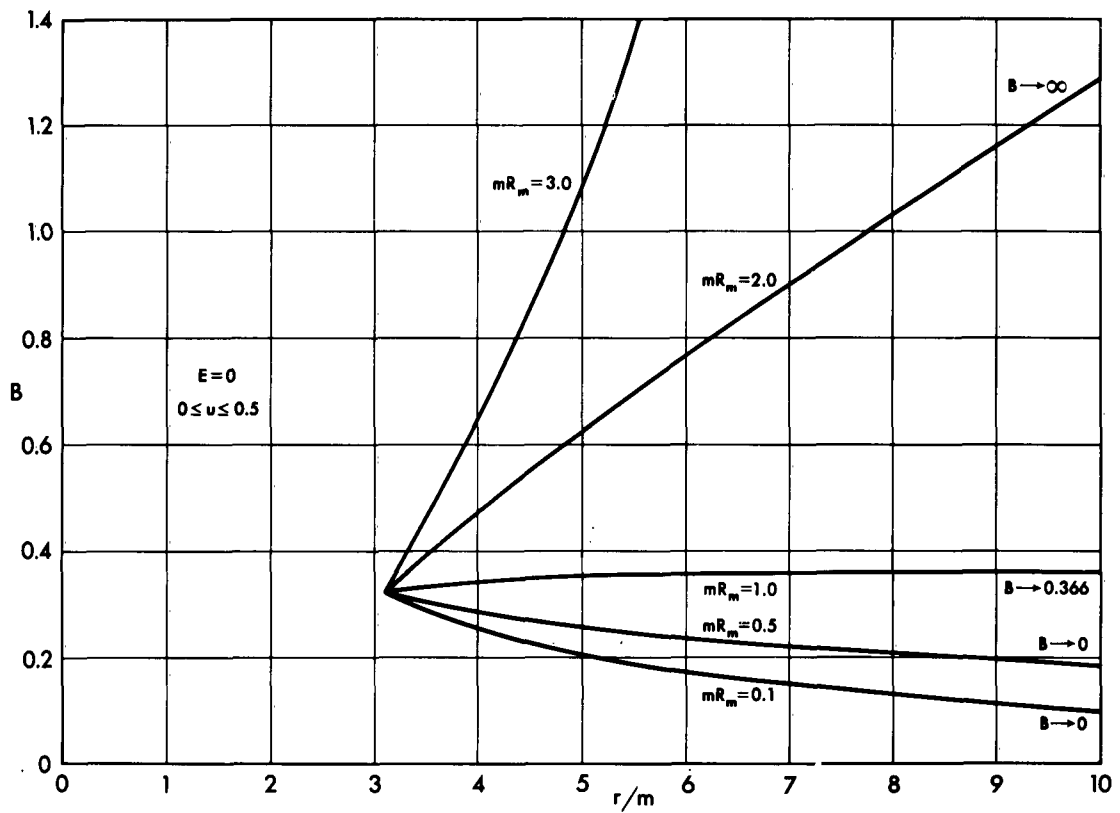
Fig. 34. Magnetic field distribution for subsonic source with E = 0.
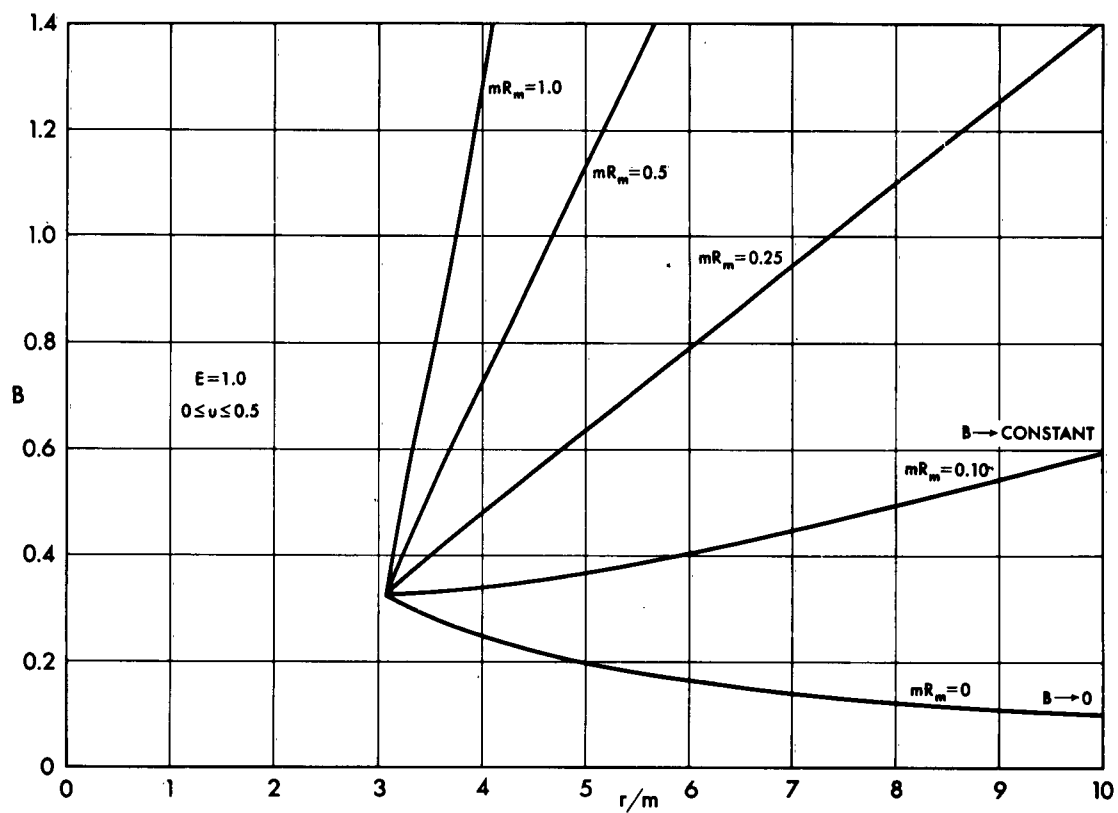
Fig. 35.   Magnetic field distribution for subsonic source with E = 1.
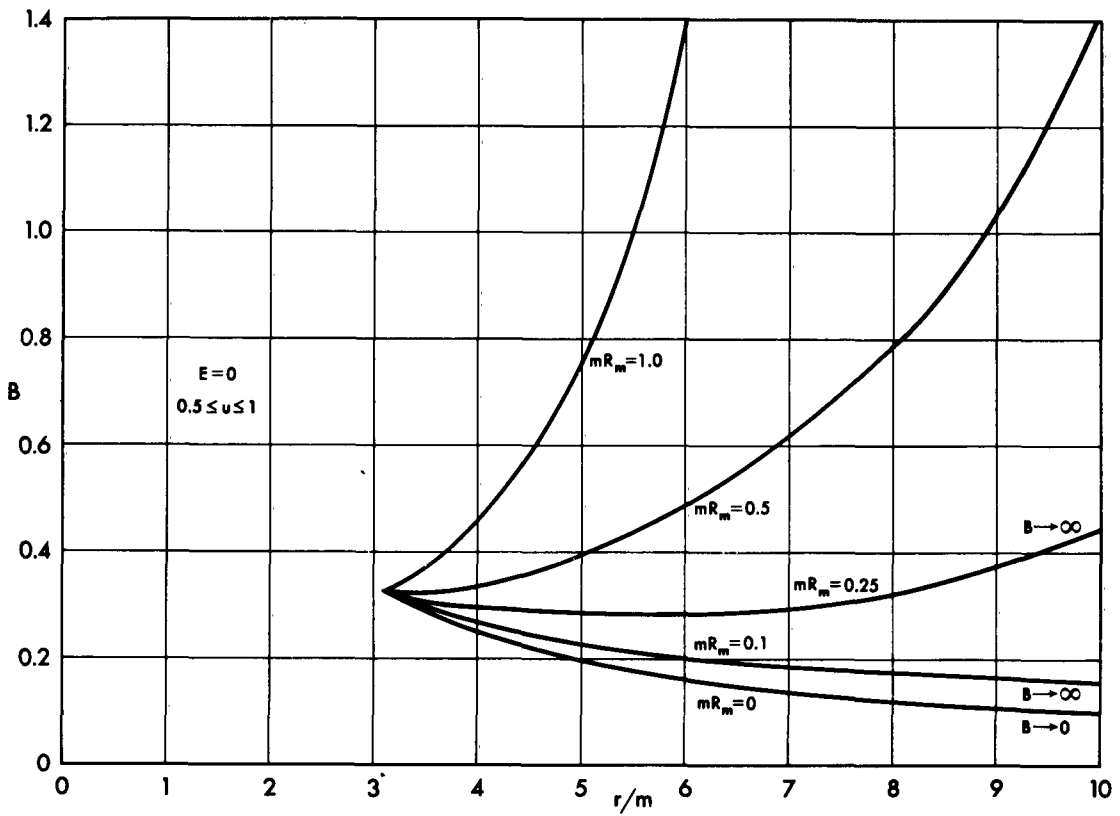
Fig. 36.   Magnetic field distribution for supersonic source with

E = 0.
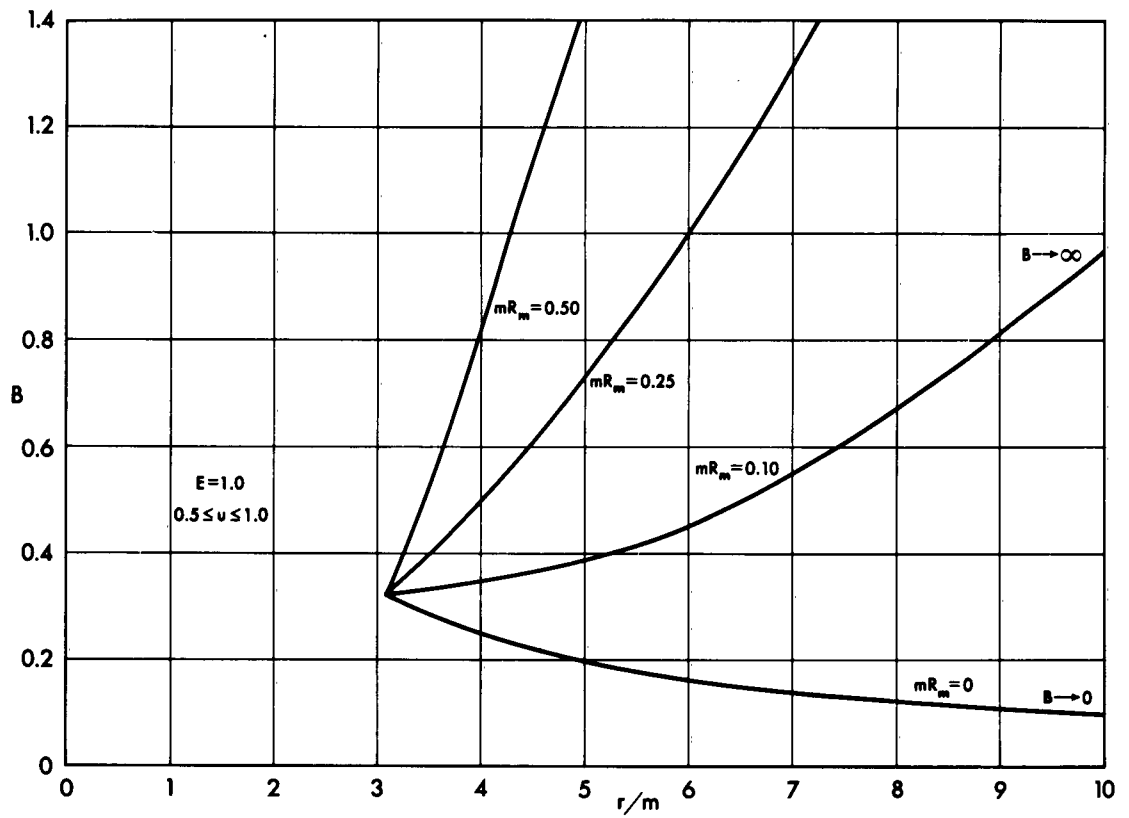
Fig. 37. Magnetic field distribution for supersonic source with
E = 1.0.
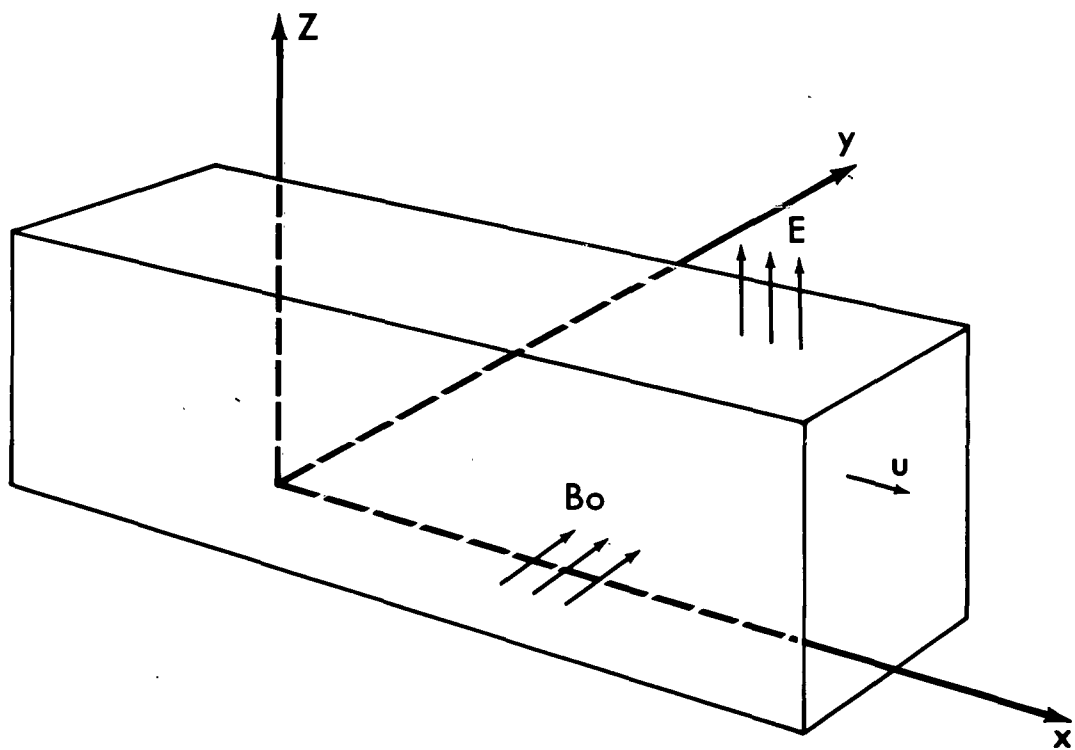
Fig. A-1. Geometry of crossed field constant area channel.
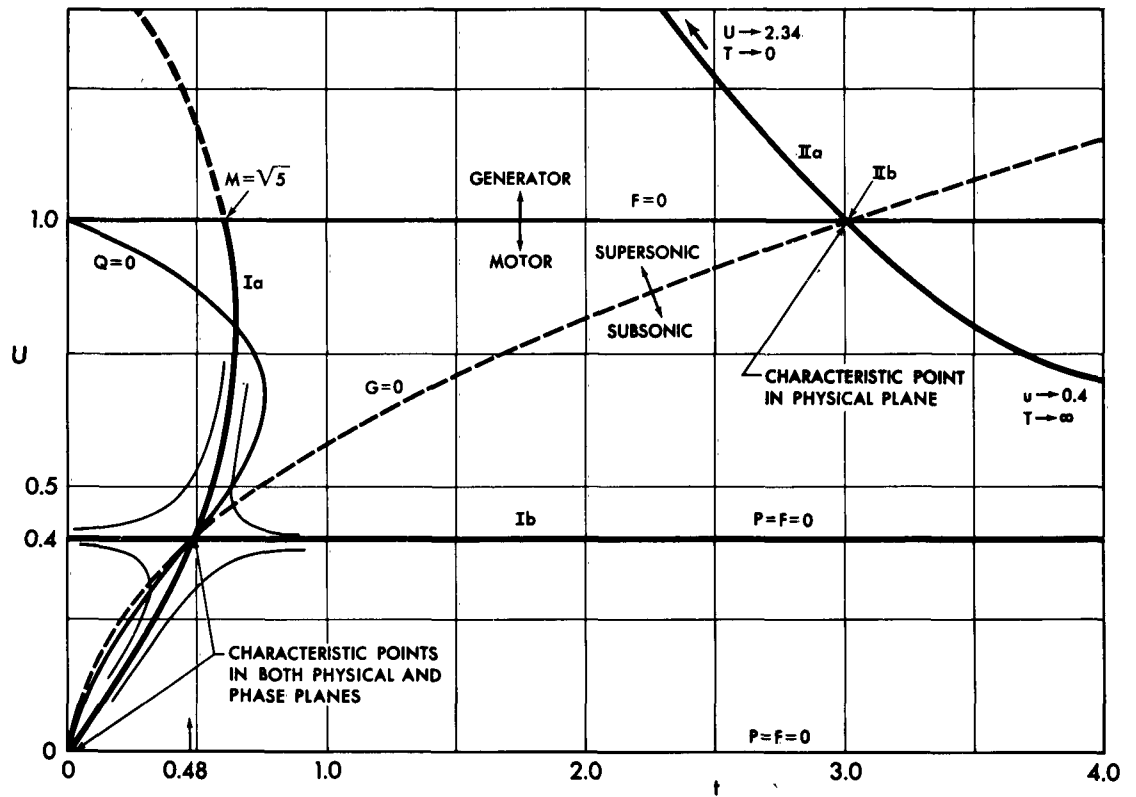
Fig. A-2. Solution of constant area channel in the phase plane.
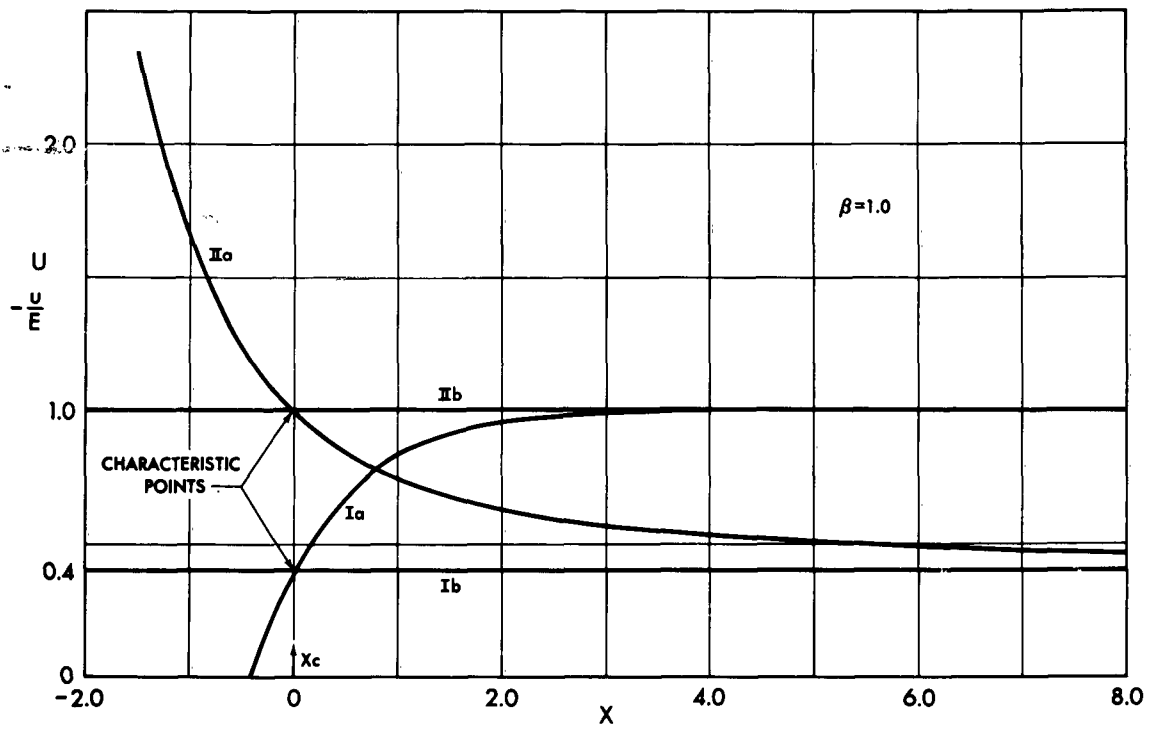
Fig. A-3. Distribution of the temperature function t.
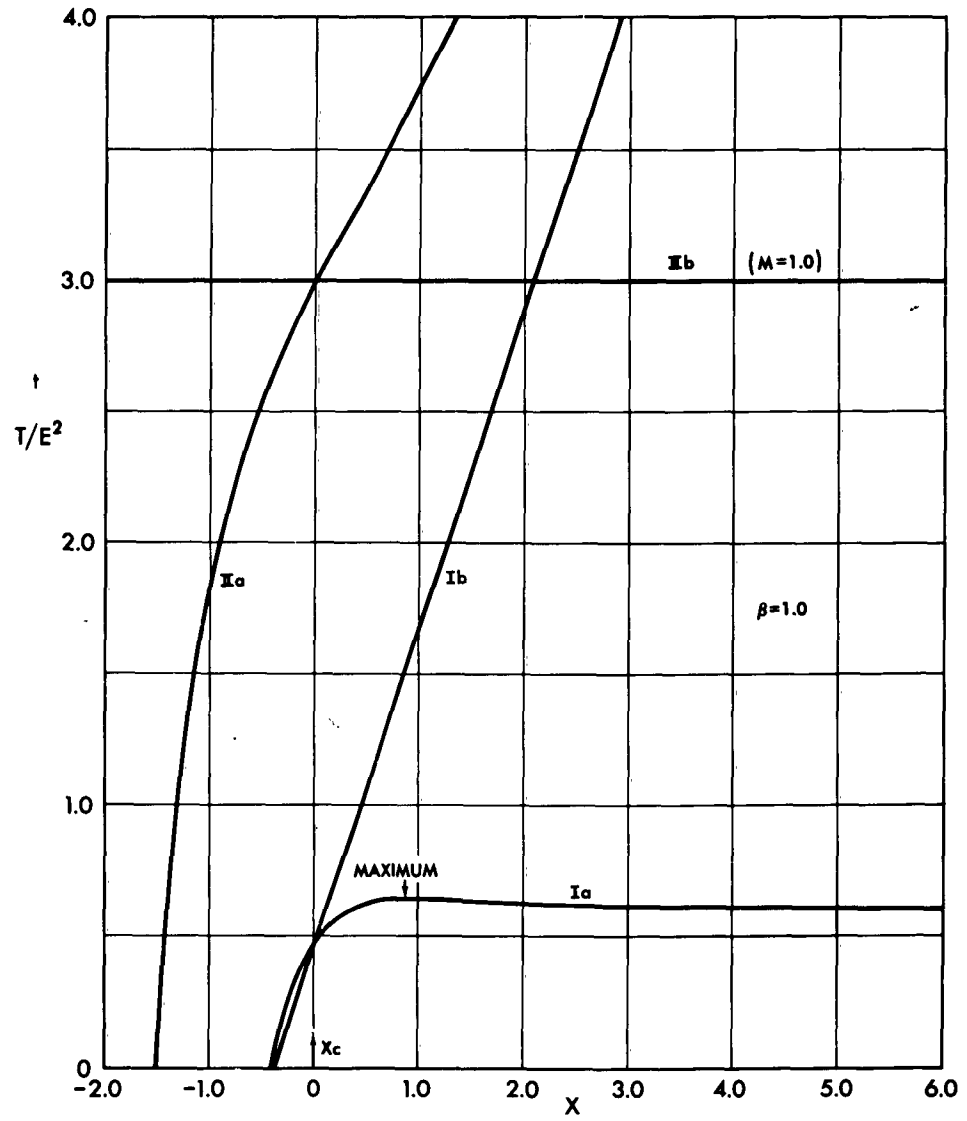
Fig. A-4.   Distribution of the velocity function U.